Structure- and Property-Based Design of Aminooxazoline Xanthenes as Selective, Orally Efficacious, and CNS Penetrable BACE Inhibitors for the Treatment of Alzheimer's Disease

Hongbing Huang,*[†,∞] Daniel S. La,*[†,∞] Alan C. Cheng,[‡,∞] Douglas A. Whittington,[‡] Vinod F. Patel,[†,△] Kui Chen,[⊥] Thomas A. Dineen,[†] Oleg Epstein,[†] Russell Graceffa,[†] Dean Hickman,[∥] Y.-H. Kiang,[#] Steven Louie,[∥] Yi Luo,[§] Robert C. Wahl,[⊥] Paul H. Wen,[§] Stephen Wood,[§] and Robert T. Fremeau, Jr.[§]

[†]Department of Medicinal Chemistry and [‡]Department of Molecular Structure, Amgen Inc., 360 Binney Street, Cambridge, Massachusetts 02142, United States

[§]Department of Neuroscience, [∥]Department of Pharmacokinetics and Drug Metabolism, [⊥]Department of HTS and Molecular Pharmacology, and [#]Department of Pharmaceutics, Amgen Inc., One Amgen Center Drive, Thousand Oaks, California 91320, United States

S *Supporting Information*

ABSTRACT: A structure- and property-based drug design approach was employed to identify aminooxazoline xanthenes as potent and selective human *β*-secretase inhibitors. These compounds exhibited good isolated enzyme, cell potency, and selectivity against the structurally related aspartyl protease cathepsin D. Our efforts resulted in the identification of a potent, orally bioavailable CNS penetrant compound that exhibited in vivo efficacy. A single oral dose of compound **11a** resulted in a significant reduction of CNS A*β*40 in naive rats.
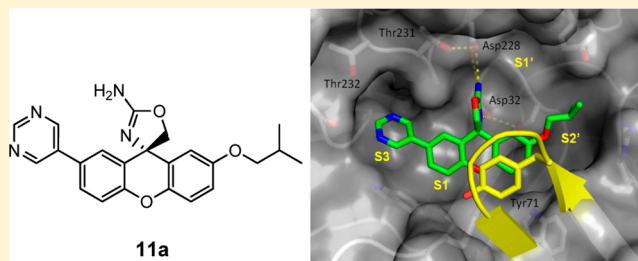
INTRODUCTION

Alzheimer's disease (AD) is the leading cause of dementia and represents a substantial unmet medical need.[1] AD is a chronic neurodegenerative disorder characterized by progressive loss of brain function, affecting memory, language skills, and bodily functions, and inevitably leads to incapacitation and death. The hallmarks of AD pathology include extracellular amyloid plaques primarily containing aggregated *β*-amyloid (A*β*) peptides derived from the *β*-amyloid precursor protein (APP), and intracellular neurofibrillary tangles containing hyperphosphorylated tau proteins.[2]

The amyloid hypothesis states that production of A*β* peptides from APP is responsible for the observed disease pathology.[3] The cleavage of APP by *β*-secretase (BACE) generates a soluble version of APP (sAPP*β*) and a resultant membrane-bound C-terminal domain. Subsequent intramembrane proteolysis of the C-terminal domain by *γ*-secretase produces amyloidogenic A*β*40 and A*β*42 peptides. A*β*42 is prone to self-assembly into fibrils and is the major A*β* component in amyloid plaques. The N-terminal domain of APP (N-APP), produced by further cleavage of sAPP*β*, has been shown to trigger neuron degeneration via caspases.[4] Therefore, an increased production of A*β* caused by the dysregulation of APP processing could induce cell death processes and disturb axonal transport. These processes ultimately lead to defects in cognition, synaptic plasticity, and the development of subsequent tau pathology. Given the critical role of BACE in APP metabolism, inhibition of BACE has gained considerable

attention as a potential disease-modifying treatment of AD.[5] In addition, the observation that BACE knockout mice lacking *β*-secretase activity develop normally and display no profound phenotype reinforces the strategy of BACE inhibition as a safe approach to the treatment and prevention of AD.[6]

Despite the identification of BACE over a decade ago and the relatively large number of preclinical programs within both academia and industry, only a handful of compounds have advanced into the clinic,[7] underscoring the difficulties with generating a safe, potent inhibitor with druglike properties suitable for targeting the central nervous system (CNS). In the arena of small molecule inhibitors of BACE, compounds from Merck, Eisai, Eli Lilly, and CoMentis have entered clinical trials.[8] The localization of BACE protein in acidic intracellular compartments poses a significant challenge for transition-state-based BACE inhibitors, as many potent enzyme inhibitors fail to show activity in cellular assays, presumably because of poor permeability or lack of sufficient binding affinity under acidic conditions.[9] Furthermore, its site of action in the CNS makes effective in vivo inhibition of BACE a pharmacokinetic challenge.[10] Several programs from the early 2000s were based on hydroxyethylamine (HEA) and hydroxyethylene (HE) structures[11] which generally suffer from low brain
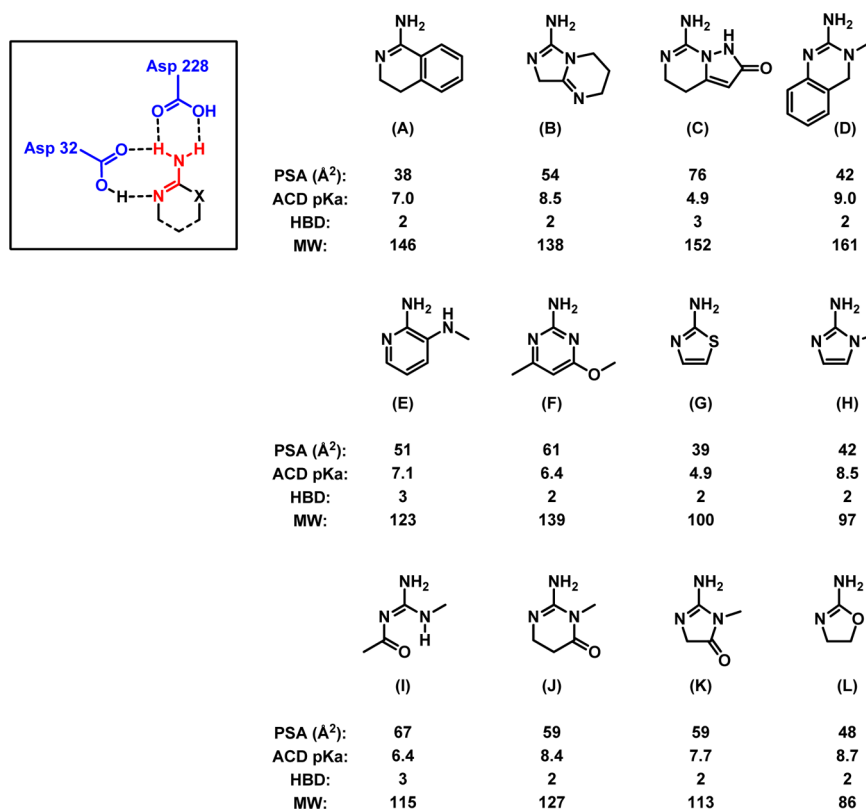
Figure 1. Calculated physiochemical properties of catalytic aspartate binding cores. PSA values were calculated in ChemDraw (version 9.0). pK_a values of structures shown were calculated using ACD LogD Suite (version 10, Advanced Chemistry Development Inc., Toronto, Canada).

Table 1. SAR of 2-Aminooxazoline BACE Inhibitors

compd	Ar	R	IC$_{50}$ (μM)[a] BACE	Cat D	cellular	HLM/RLM (μL min^{-1} mg^{-1})[b]	P_{app} (10^{-6} cm/s)[c]	ER[c,d]
1	5-Cl-2-F-Ph	Me	1.95 ± 0.10	10.7 ± 3.75	12	54/>399	4.2	0.6
2	3-Cl-Ph	Me	2.06 ± 0.16	12.7 ± 0.19	18	39/>399	3.4	0.7
3	pyridin-3-yl	Me	7.46 ± 0.57	>100	5.5	110/>399	36	12
4	pyrimidin-5-yl	Me	11.4 ± 0.35	>100	13	54/300	40	8.8
5	6-F-pyr-3-yl	Me	8.20 ± 0.66	47.7 ± 6.41	8.3	51/280	32	5.7
6	2-F-pyr-3-yl	Me	2.85 ± 0.17	12.6 ± 0.63	5.1	165/>399	15	1.6
7	(R)-2-F-pyr-3-yl	CHF$_2$	1.21 ± 0.67	7.65 ± 5.68	1.7	36/38	12	1.4

[a]Values represent the mean values of at least two experiments ± SD. Values without SD are for a single determination only. [b]Compounds were incubated with microsomes for 30 min at 1 μM. [c]Parental LLC-PK1 cell line. [d]B/A to A/B ratio.

penetration, poor oral bioavailability, and susceptibility to p-glycoprotein (PGP) transport.[5]

More recently, 2-aminoheterocyclic inhibitors of BACE have emerged as promising leads.[12] These classes of compounds are reliant on a two-point contact between an "amidine" type functional group and the catalytic aspartates (32 and 228) of the active site (see boxed structure of Figure 1). Publicly disclosed examples include compounds with aminopyridines, aminohydantoins, and aminoquinolines as the Asp-binding motif.[13] While these compounds tend to have lower molecular weight compared to HEA inhibitors, they often suffer from PGP efflux, poor brain exposure, and undesired activity on the hERG ion channel. Herein, we describe our initial efforts

toward rational design of aminooxazoline xanthenes as potent, orally efficacious, and CNS penetrant inhibitors of BACE.

RESULTS AND DISCUSSION

Our initial design approach took into consideration computed properties that could improve CNS exposure: polar surface area (PSA), pK_a, and molecular weight.[14,15] As shown in Figure 1, computational analysis of core Asp binding moieties from both our internal efforts and the literature revealed that PSA values range from 38 to 67 Å^2 and ACD calculated pK_a values range from 4.9 to 9.0.[16] While the pK_a values of the core structures will be affected by substitution, the calculated values aided prioritization of core structures relative to each other.[17]

Presumably, the high pK_a values exhibited by these 2-aminoheterocycles were designed to complement the acidity of the catalytic aspartates[18] and to accommodate the acidic (pH ≈ 4.5) operating environment of BACE.[19] Studies at Merck have demonstrated that pK_a plays a critical role in enzymatic binding and cellular potency.[20] They demonstrated that an inhibitor containing the more basic 1-methyl-2-aminoimidazole (H) exhibited improved potency relative to that bearing an aminothiazole (G).[20a] The improvement was proposed to be a result of increasing pK_a which should be on the order of ~3.6 log units. Design criteria, however, also targeted heterocycles with pK_a values of <10 in order to achieve high oral bioavailability.[21] We were aware that basic amidines often required a prodrug strategy in order to achieve oral bioavailability.[22]

Mindful of these considerations, the oxazoline Asp-binding group (L, Figure 1) was chosen for further evaluation based on its low molecular weight (86 amu), low PSA (48 Å[2]), and relatively high pK_a (8.7). In addition, the hydrogen bond donor (HBD) count was limited to 2 in consideration of the properties required for good CNS exposure. Furthermore, in contrast to cores D–I, the sp[3] hybridization of the center adjacent to the "amidine" functional group (red in Figure 1) in the oxazoline ring allowed for stereocontrolled projection of substituents into S1 and S2′ (vide infra).

A series of racemic biaryl spiro-aminooxazolines was prepared (Table 1). All compounds were evaluated for their inhibitory activity against BACE in a homogeneous fluorescence resonance energy transfer (FRET) assay. We sought to attain a high level of selectivity against other aspartyl proteases in order to develop BACE inhibitors with a good safety profile. As an initial test of selectivity, we evaluated compounds against the closely related aspartyl protease cathepsin D (Cat D). For advanced compounds, selectivity screening across a broader panel of aspartyl proteases was undertaken. The cellular potency of the compounds was assessed by measuring the inhibition of $A\beta_{40}$ production in HEK293 cells expressing amyloid precursor protein. Initial SAR studies revealed that only modest potency was achievable with various substituted aryl rings. In general, substituted phenyl analogues exhibited no cellular potency with a few exceptions. IC_{50} values in the single digit micromolar range were observed with aryl rings containing a 2-fluoro substituent (compounds **1** and **6**). In addition, single digit micromolar cell potencies were observed with the introduction of a pyridyl ring, presumably because of productive interactions with the water H-bond found in the S3 pocket (shown in Figure 2). The data also indicated that Cat D selectivity was potentially emerging. For example, greater than 10-fold selectivity was observed with compound **3**.

Most of the compounds within this series demonstrated high clearance when incubated with rat liver microsomes and poor permeability in LLC-PK1 cells as represented by compounds **1** and **2** (Table 1). By comparison, compound **6** showed improved permeability while maintaining a low efflux ratio. Unfortunately, the microsomal turnover of **6** remained high. A vast improvement in RLM metabolic stability was observed with compound **7**. The stability imparted by the difluoromethoxy modification suggests that demethylation is the main route of metabolism during RLM incubation for compounds **1**−**6**. Encouragingly, **7** showed good permeability and PGP efflux was low (ratio of 1.4). In addition **7** was chemically stable under acidic conditions. For instance, the purity of **7** remained unchanged even when stirred in 2.0 N HCl at room
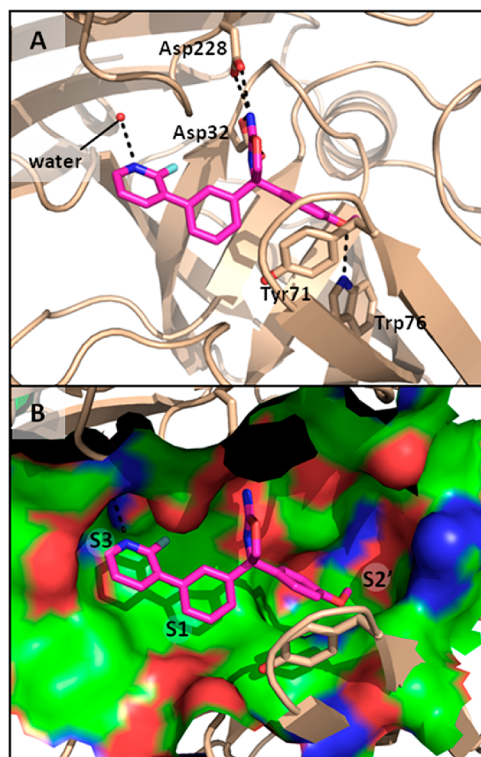

Figure 2. X-ray cocrystal of aminooxazoline **6** in BACE.

temperature for 18 h. While increasing the potency of this class remained an objective, the promising in vitro PK data indicated that the oxazoline core had potential to be CNS penetrant and metabolically stable, given its permeability, low efflux ratio, and low microsomal turnover.

To better understand the origins of the moderate potency and to gain insight to possible interactions that could be exploited to improve potency, a cocrystal structure of compound **6** bound to BACE was obtained (Figure 2). A hydrogen bonding network and electrostatic interaction between the catalytic diad (Asp228 and Asp32) and the aminooxazoline core were observed. In addition, the phenyl-pyridyl moiety occupied the S1−S3 pocket, with the pyridyl nitrogen accepting a hydrogen bond from the backbone N−H of Ser229 through a bridging water molecule. The dihedral angle between the phenyl ring and the pyridyl ring was about 60°, suggesting that the 2-fluoride substitution not only served to engage in van der Waals contacts but also may have reinforced this conformation, thereby imparting the increased potency found with **1** and **6**. On the "prime" side of the aminooxazoline, an edge-to-π face interaction was observed between the phenyl ring and Tyr71 with a distance of about 3.8 Å. In addition, the ether of **6** was a hydrogen bond acceptor with the side chain of Trp76.

From the structure−activity relationship (SAR) of HEA inhibitors, we had previously discovered that hydrophobic moieties placed in the S2′ pocket can provide a significant potency increase.[23] For instance, a cocrystal structure of **8a** bound to BACE showed that the neopentyl group extends into the S2′ pocket (Figure 3A). An increase in van der Waals contacts and hydrophobic interactions with the protein in this region results in compounds **8b** and **8c** (R^2 = neopentyl and isobutyl, respectively) gaining 1000-fold in enzyme potency and 200-fold in cell potency compared to **8f** (R^2 = H) (Table 2).
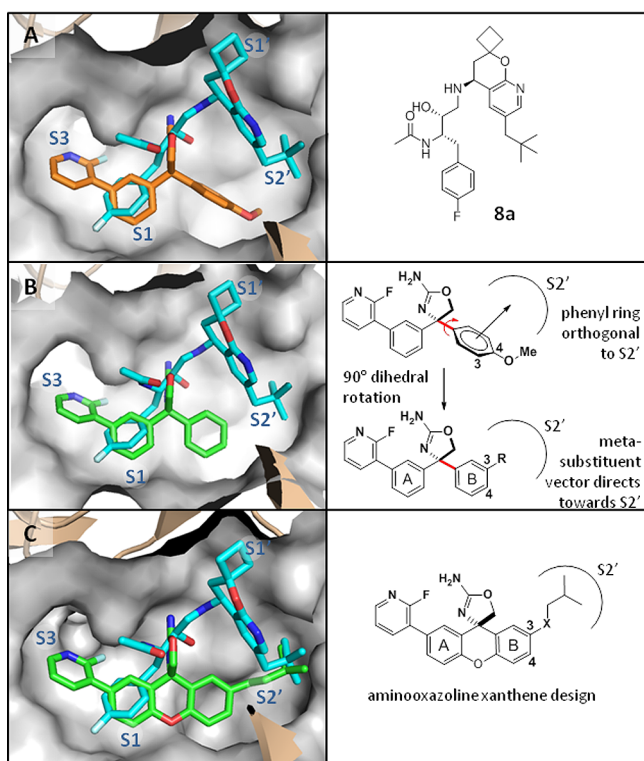
Figure 3. Design of aminooxazoline xanthenes: (A) overlay of X-ray BACE binding structure of HEA compound **8a** and 2-aminooxazoline **6**; (B) model of **6** where right side phenyl group is rotated by 90°; (C) proposed binding model of aminooxazoline xanthene.

Table 2. Examples of HEA SAR for P2′ Substituents

| | | | IC$_{50}$ (μM)^a | |
compd	R$_1$	R$_2$	BACE	cellular
8a	F	(CH$_3$)$_3$CCH$_2$	0.005 ± 0.002	0.01 ± 0.006
8b	H	(CH$_3$)$_3$CCH$_2$	0.006 ± 0.006	0.003 ± 0.004
8c	H	(CH$_3$)$_2$CHCH$_2$	0.005 ± 0.002	0.004 ± 0.002
8d	H	CH$_3$CH$_2$	0.091 ± 0.056	0.039 ± 0.023
8e	H	Cl	0.957 ± 0.043	1.88
8f	H	H	5.28 ± 1.18	0.804

^{a}Values represent the mean values of at least two experiments ± SD. Values without SD are for a single determination only.

We envisioned that by exploiting similar interactions in the S2′ pocket, we could enhance the potency of our aminooxazoline compounds. A key insight was the realization that rotation of the right-most phenyl ring (ring B) by ~90° would allow direct access to S2′ by a meta substituent (Figure 3B). To lock this conformation, we designed a xanthene based 2-aminooxazoline core (Figure 3C). By linkage of the adjacent phenyl rings through an oxygen atom, the rigid tricycle structure positions the substituent at the 3-position of the xanthene toward the S2′ site; this rigid structure also decreases the number of rotatable bonds, thereby potentially decreasing the binding entropic penalty.[24] In addition, aryl substitution at the

meta position of the A ring would be appropriately positioned to exploit the S1/S3 pockets of the enzyme.

The S1 pocket consists mostly of hydrophobic residues; hydrophobic interactions with the enzyme in this region contribute significantly to potency. Aromatic groups, such as a phenyl ring, have been shown as good ligands for S1.[12,25] This pocket is adjacent to the S3 pocket which also consists of a largely hydrophobic environment. The S3 site accommodates large hydrophobic ligands through van der Waals contacts with the enzyme.[26] The hydrophobic environment stretching from S1 to S3 presents an attractive opportunity to occupy the S3 binding pocket with a group extending from the S1 moiety.[27] We envisioned the A ring of the xanthene core could occupy the S1 hydrophobic pocket, and the meta position of the A ring would project a substituent toward the nearby S3 site.

As a starting point, we decided to pursue a library of meta,meta bis-substituted aminooxazoline xanthenes (AOX) **9** via parallel synthesis. To test our hypothesis, we first installed a methoxy group at the 3 position of the B ring of the xanthene core to partially occupy the S2′ pocket with the intention of exploring the prime side pockets at a later stage. The methoxy group could serve as an indicator of whether hydrophobic interactions in the region could bring in better potency compared to the biarylaminooxazoline **6**. To maximize the potential for optimal interactions with the protein, we first investigated phenyl rings with a variety of substituents for potential hydrophobic interactions with the S3 pocket.

The SAR is summarized in Table 3. Monosubstitution at the ortho- or para-position of the phenyl ring did not improve potency; ortho-substitution alone proved to be detrimental to the potency (**9b**, **e**). At para-positions of the phenyl ring, small groups such as a chlorine atom or a methyl group provided similar potency as an unsubstituted phenyl ring (**9d,g**). Larger groups such as a trifluoromethoxy group (**9h**) decreased potency. Meta-substitution proved to have a great impact on potency; **9f** (3-Cl-phenyl) is 10-fold more potent than **9c** (3-Me-phenyl) and **9i** (3-CF$_3$O-phenyl). The disubstituted phenyl rings with a fluorine atom at the 2-position were beneficial to potency. With a substituent at the 5-position of the 2-fluorophenyl ring, **9l** (2-F-5-Cl-phenyl) and **9n** (2-F-5-MeO-phenyl) demonstrated submicromolar enzymatic potency (IC$_{50}$ = 0.28 and 0.74 μM, respectively). Moving the methoxy group to the 3-position resulted in another inhibitor **9m** (2-F-3-MeO-phenyl) with good activity (IC$_{50}$ = 0.9 μM). Substitution at the 4-position of the phenyl ring was not tolerated, as **9o** (2-F-4-Me-5-Cl-phenyl) lost significant potency compared to **9l**.

To aid further design, a cocrystal structure of **9l** bound to BACE was solved at 1.95 Å resolution (Figure 4A). Although racemic **9l** was used for crystallography, only the (S)-enantiomer crystallized with the protein. By analogy with compound **6**, 2-aminooxazoline **9l** interacts with the catalytic Asp32 and Asp228 through a hydrogen bond network. As anticipated, the A ring of the xanthene core occupies the S1 pocket, from which the 2-fluoro-5-chlorophenyl group extends into the S3 pocket where the chlorine atom makes hydrophobic interactions with the backbone of residues Gly13, Gly230, and Thr231. It seems likely that the same hydrophobic interactions also accounted for the good potency of **9f**. Notably a water molecule, which is tightly bound to the carbonyl groups of protein residues Ser229 and Thr231, is also close to the chlorine atom in this region. In addition, the xanthene tricyclic moiety of **9l** makes a π-stacking interaction with Tyr71 from the flap region of BACE. Furthermore, while the methoxy

Table 3. SAR of Xanthene BACE Inhibitors

compd	Ar	IC$_{50}$ (μM)[a] BACE	cellular	Cat D
9a	phenyl	1.18 ± 0.11	2.52 ± 1.79	>40
9b	2-Me-phenyl	7.02 ± 4.28	4.22	30.9 ± 8.6
9c	3-Me-phenyl	1.67 ± 1.52	4.54 ± 2.43	26.9 ± 2.0
9d	4-Me-phenyl	1.78 ± 0.21	3.63	>40
9e	2-Cl-phenyl	4.88 ± 3.7	2.47	16.8 ± 5.0
9f	3-Cl-phenyl	0.13 ± 0.03	2.51 ± 0.90	35.7 ± 4.7
9g	4-Cl-phenyl	2.02 ± 0.003	2.42 ± 1.75	>40
9h	4-CF$_3$O-phenyl	5.06 ± 3.45	3.69 ± 2.77	>40
9i	3-CF$_3$O-phenyl	2.76 ± 2.43	6.41 ± 4.37	20.1 ± 3.9
9j	2-F-3-Cl-phenyl	1.17 ± 1.09	6.75 ± 1.4	13.7 ± 3.4
9k	2-F-4-Cl-phenyl	1.56 ± 0.34	2.24 ± 2.51	28.5 ± 5.5
9l	2-F-5-Cl-phenyl	0.28 ± 0.10	4.29 ± 4.16	3.7 ± 1.7
9m	2-F-3-MeO-phenyl	0.90 ± 0.88	2.23 ± 0.89	37.3 ± 1.8
9n	2-F-5-MeO-phenyl	0.74 ± 0.71	3.72 ± 1.84	13.7 ± 0.8
9o	2-F-4-Me-5-Cl-phenyl	3.21 ± 2.01	2.98	13.8 ± 4.3
9p	2-F-pyridin-3-yl	0.80 ± 0.86	2.0 ± 1.88	16.0 ± 6.8
9q	4-F-pyridin-3-yl	0.90 ± 0.09	1.33 ± 0.81	>40
9r	2-Cl-pyridin-4-yl	2.11 ± 1.62	5.80 ± 4.49	44.2 ± 4.08
9s	pyridin-4-yl	3.90 ± 0.14	2.82	>40
9t	(rac)-pyrimidin-5-yl	0.41 ± 0.4	1.43 ± 0.38	37.0 ± 7.4
9u	(S)-pyrimidin-5-yl	0.107 ± 0.024	0.534 ± 0.325	29.7 ± 1.48
9v	(R)-pyrimidin-5-yl	10.40 ± 0.86	ND	>40

[a]Values represent the mean values of at least two experiments ± SD. Values without SD are for a single determination only. ND = not determined.
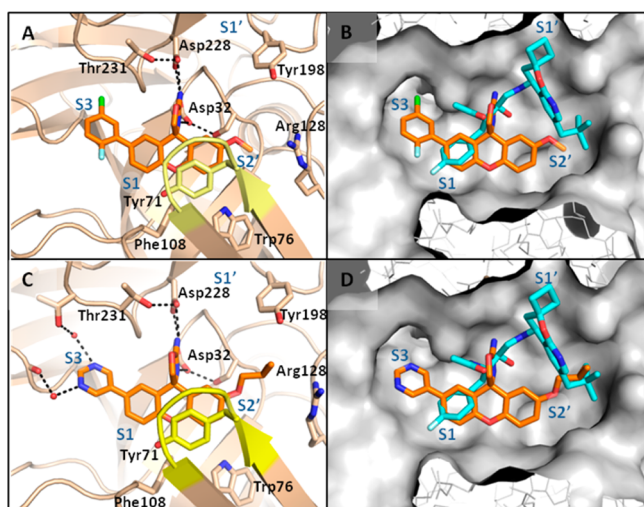
Figure 4. X-ray cocrystal structures: (A) 9l bound to BACE protein; (B) 9l bound to BACE protein with superimposed HEA 8a in blue; (C) 11a bound to BACE protein; (D) 11a bound to BACE protein with superimposed HEA 8a in blue.

group in 6 hydrogen-bonds to Trp76, the rigid tricyclic ring projects the methoxy group of 9l to the upper portion of the S2′ pocket. The structure confirmed our hypothesis and indicated that potency could be improved by extending off the methoxy group and deeper into the S2′ pocket. The presence of water molecules in the S3 pocket prompted us to investigate the possibility of gaining affinity by interacting with the enzyme backbone residues through water bridged hydrogen bond interactions. A variety of heteroaromatic groups were then explored to fill the S3 pocket (Table 3, compounds 9p−v).
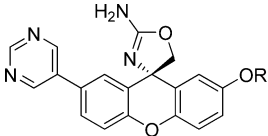
Heteroaromatic groups, such as substituted pyridyl and pyrimidyl groups, displayed promising inhibitory activity. Not surprisingly, the position of the heteroatom on the ring affects potency. For instance, pyridine-3-yl is superior to pyridine-4-yl (Table 3, compounds 9p−s). Notably, the enzyme potency of 9t (IC$_{50}$ = 0.41 μM) represented a 28-fold increase compared to its biarylaminooxazoline congener 4. The two enantiomers of 9t were obtained in excellent optical purity (>99% ee) by chiral HPLC separation. The (S)-enantiomer 9u was significantly more potent (10-fold) than the (R)-isomer 9v and is consistent with the cocrystallization of (S)-9l.

Table 4. Compound Profile of Selected Compounds

compd	MW	PSA (Å^2)	cLogP	HBD	rotatable bonds	BE	RLM/HLM (μL min^{-1} mg^{-1})[a]	hER[b,c]	P_{app} (10^{-6} cm/s)[c]
9f	393	66	5.07	2	2	0.33	200/390	1.0	5.4
9l	411	66	5.21	2	2	0.31	170/130	0.5	5.7
9t	360	91.9	1.90	2	2	0.32	52/80	3.0	17

[a]Compounds were incubated with microsomes for 30 min at 1 μM. [b]B/A to A/B ratio. [c]Parental LLC-PK1 cell line.

Table 5. SAR of Xanthene BACE Inhibitors

| compd | R | IC$_{50}$ (μM)^a | | | P_{app} (10^{-6} cm/s)^b | hER^{b,c} |
		BACE	cellular	Cat D		
9u	Me	0.107 ± 0.024	0.534 ± 0.325	29.7 ± 1.48	17	2.2
10a	Pr	0.016 ± 0.003	0.052 ± 0.013	9.12 ± 4.29	14	1.5
11a	*i*-Bu	0.008 ± 0.0003	0.036 ± 0.007	4.47 ± 0.584	9.1	0.9

^{a}Values represent the mean values of at least two experiments ± SD. ^{b}Parental LLC-PK1 cell line. ^{c}B/A to A/B ratio.

Table 6. Pharmacokinetic Profile of Selected Compounds in Rats

compd	HLM^a (μL min^{-1} mg^{-1})	RLM^a (μL min^{-1} mg^{-1})	CL^b (L h^{-1} kg^{-1})	$V_{ss}{}^b$ (L/kg)	$T_{1/2}{}^b$ (h)	AUC$_{inf}{}^c$ (μM·h)	F^c (%)
9u	97	22	2.86	2.76	3.7	20.9	260
10a	55	21	4.92	9.37	3.2	5.66	110
11a	19	20	1.08	3.49	3.2	7.29	31

^{a}Compounds were incubated with microsomes for 30 min at 1 μM. ^{b}2 mg/kg iv dose (solution in 100% DMSO). ^{c}10 mg/kg oral dose (solution in (1% Tween 80)/(2% HPMC)).

Encouragingly, **9u** also demonstrated 270-fold selectivity against the closely related aspartyl protease Cat D. These compounds also consistently demonstrated ≤5-fold enzyme to cell shift. For instance, the most potent enzyme inhibitor **9u** recorded a cellular IC$_{50}$ of 0.53 μM, a cell shift of 5-fold.

Selected compounds were further profiled to get an understanding of their ability to penetrate the blood−brain barrier (BBB) (Table 4). Compounds **9f**, **9l**, and **9t** displayed favorable calculated physiochemical properties required for CNS drugs: a low molecular weight (<400 Da), few hydrogen bond donors (2), limited rotatable bonds (2), and low polar surface area.[15,28] In addition, these compounds do not appear to be substrates of the PGP transporter (efflux ratios of 1.3, 0.5, and 3.0, respectively). With a cLogP of 1.9, compound **9t** demonstrated good apparent permeability (P_{app} of 17.2 × 10^{-6} cm/s). On the other hand, the more lipophilic compounds **9f** and **9l** were less permeable (P_{app} of 5.4 × 10^{-6} and 5.7 × 10^{-6} cm/s, respectively), which might contribute to their high enzyme to cell shift (Table 3). Furthermore, **9t** demonstrated better intrinsic stability in liver microsomes compared to **9f** and **9l**. Because of overall attractive physiochemical properties of **9t** for CNS penetration and the overall superior properties brought by the pyrimidin-3-yl group, we chose to investigate this series further.

To improve the potency of **9t**, we pursued the second part of our hypothesis, which was to gain affinity by filling the S2′ pocket through extension of the methoxy group. Specifically, we investigated interactions with the S2′ pocket by exploring substitution of the aryl ether in **9**. As anticipated, filling the S2′ pocket with bulkier hydrophobic groups provided a significant increase in enzymatic inhibition and cellular potency (Table 5). Increasing the size from a methyl group to an *n*-propyl substituent resulted in a more than 10-fold increase in both enzyme and cell activity. A further increase in size to an isobutyl group led to an additional ∼2-fold enhancement in potency. These initial results confirmed our hypothesis that engaging hydrophobic interactions in S2′ pocket could boost potency. Encouragingly, compounds **10a** and **11a** maintained good permeability and a low PGP-mediated efflux (Table 5). In addition to the improved BACE potency, another appealing

outcome of extending deep into the S2′ pocket is the enhanced selectivity against Cat D. For example, Cat D selectivity increased from 270-fold for **9t** to 560-fold for **11a**.

A cocrystal structure of **11a** bound to BACE protein was obtained at 2.1 Å resolution (Figure 4C). Compound **11a** bound to the BACE protein similarly to previous structures. The aminooxazoline interacts with the catalytic aspartate diad in a fashion similar to **9l**, with the xanthene moiety π-stacking with Tyr71 and the pyrimidine ring of **11a** occupying the S3 pocket. Unlike the hydrophobic interactions made by the 2-F-5-Cl-phenyl group of **9l** in the S3 region, the pyrimidine of **11a** interacts with BACE protein via two water-bridged hydrogen bond networks. One N-atom of the pyrimidine ring interacts with the side chain of Thr232 through a water-mediated hydrogen bond. In the same region of the crystal structure of **9l** bound to BACE, a water molecule appears to tightly bind to Thr232 and Ser229 via hydrogen bonds. In the structure of **11a** and BACE, the water molecule has been displaced outside hydrogen bonding distance from the residue Ser229. The other N-atom of the pyrimidine ring interacts with the backbone carbonyl of Gly11 through a second water bridged H-bond network. As expected, the isobutyl group of compound **11a** extends deeply into the upper region of the S2′ pocket. An overlay of cocrystal structures of **11a**/BACE with **8a**/BACE shows clearly that the isobutyl group of **11a** occupies the same space as the neopentyl group of **8a** (Figure 4D).

With potent and selective BACE inhibitors **10a** and **11a** in hand, we sought to understand the PKDM properties of these fully elaborated aminooxazoline xanthenes (Table 6). Although the hepatic intrinsic clearance was relatively low, in vivo clearance (CL) was much higher than would be predicted.[29] For instance, while compounds **9u**, **10a**, and **11a** had similar stability in rat liver microsomes, compounds **9u** and **10a** displayed high in vivo clearance while **11a** demonstrated moderate clearance.[30] The oral bioavailability of these compounds was consistent with the moderate apparent permeability.[31] Furthermore, these compounds were poor PGP substrates, with each having a low efflux ratio (<3). Because of its good overall PK and potent cell activity,
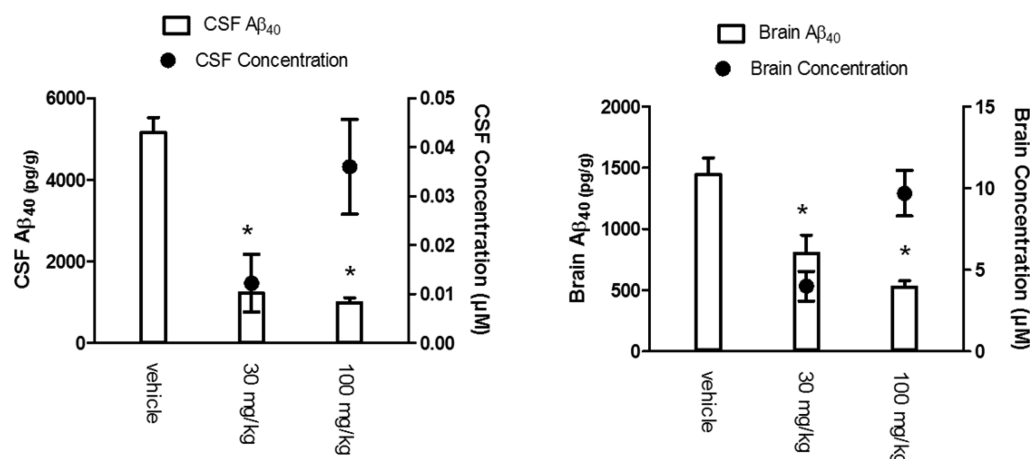
Figure 5. $A\beta_{40}$ reduction in wild type rats with **11a** at 4 h (30 and 100 mg/kg, po): (∗) $P < 0.0001$.

Table 7. In Vivo $A\beta_{40}$ Reduction in Wild Type Rats with 11a at 4 h (30 and 100 mg/kg, po)

dose[a] (mg/kg)	% inhibition in CSF	[CSF] (μM)	[CSF]/(cell IC_{50})	% inhibition in brain	[brain] (μM)	[plasma]$_{total}$ (μM)	[plasma]$_{unbound}$ (μM)
30	76	0.012	0.3	45	4.0	3.6	0.071
100	81	0.036	0.9	63	9.7	6.1	0.12

[a]Dosed as a solution in mg/kg oral dose (solution in (1% Tween 80)/(2%HPMC)).

Scheme 1. Synthesis of Biaryl Aminooxazoline BACE Inhibitors[a]
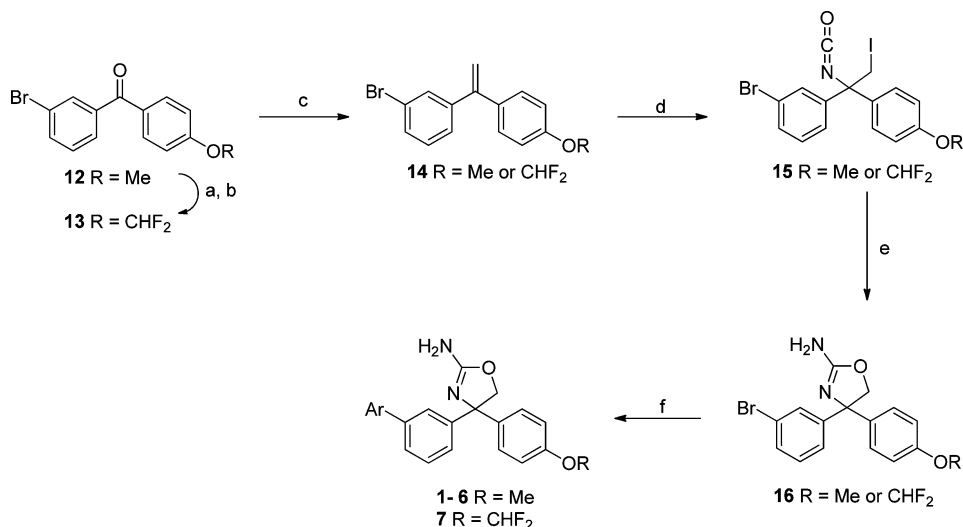
[a]Reagents: (a) BBr$_3$, CH$_2$Cl$_2$, 76%; (b) 2-chloro-2,2-difluoroacetic acid, K$_2$CO$_3$, H$_2$O, DMF, 72%; (c) PPh$_3$CH$_3$Br, n-BuLi, THF, 99%; (d) AgNCO, I$_2$, THF; (e) NH$_4$OH, acetone, 75% over two steps; (f) Ar(BOH)$_2$, Pd(PPh$_3$)$_4$, DME.

compound **11a** was chosen to study the effect of BACE inhibition on levels of $A\beta_{40}$ in the brain.

The pharmacodynamic assay was conducted in naive male Sprague−Dawley rats that were administered a single oral dose of compound **11a** at either 30 or 100 mg/kg. $A\beta$ levels and drug concentrations were measured at 4 h in the brain and CSF. Compound **11a** exhibited a significant reduction of $A\beta_{40}$ in the central nervous system (Figure 5). The brain−blood ratios of **11a**, 1.1 at 30 mg/kg and 1.6 at 100 mg/kg, suggest that the compound readily passes the blood−brain barrier (Table 7). **11a** significantly inhibited $A\beta_{40}$ production in both CSF (76%) and brain (45%) at 30 mg/kg relative to the vehicle-treated animals. At 100 mg/kg, the inhibition of $A\beta_{40}$ production was slightly improved in CSF (81%) and a more robust $A\beta_{40}$ reduction was seen in brain (63%). The degree of

$A\beta_{40}$ reduction in the CSF and brain improved with the increased exposure in the corresponding compartments (Table 7, Figure 5).

■ CHEMISTRY

The synthesis of biaryl aminooxazolines is outlined in Scheme 1. Starting with commercially available ketone **12**, demethylation mediated by BBr$_3$ followed by difluoromethylation of the resulting alcohol afforded diaryl ketone **13**. Subsequent Wittig olefination of **12/13** afforded **14**. Addition of in situ generated iodine isocyanate to **14** yielded iodide **15** which was cyclized to the penultimate aminooxazoline bromide **16** in good yield. This five-step protocol was reliable and scalable allowing for quick access to precursor **16** which was elaborated to compounds **1−7** through Suzuki coupling.

Scheme 2. Synthesis of 2-Aminooxazoline Xanthenes[a]
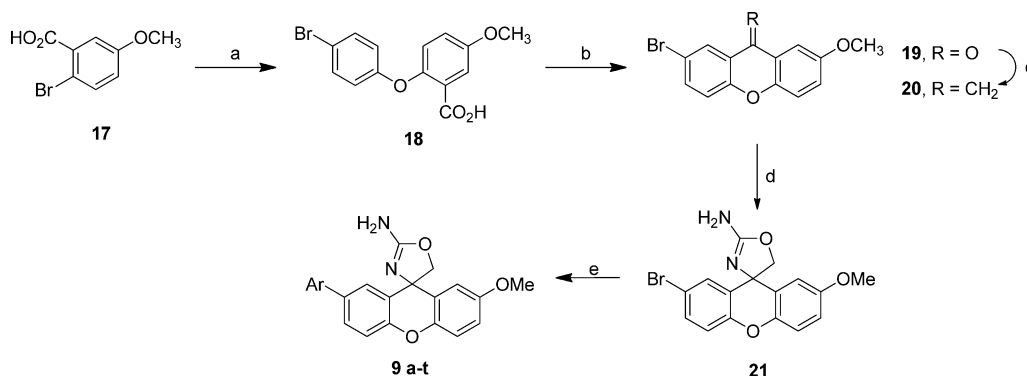
[a]Reagents: (a) 4-bromophenol, Cu(OTf)$_2$, Cs$_2$CO$_3$, cat. EtOAc, toluene, 110 °C, 68%; (b) H$_2$SO$_4$, 60 °C, 84%; (c) trimethylsilylmethyllithium, THF, −78 °C; then AcCl, 23 °C; (d) I$_2$, AgNCO, Et$_2$O; then NH$_4$OH, THF, 69%; (e) ArB(OH)$_2$, Pd(PPh$_3$)$_4$, aq Na$_2$CO$_3$, dioxane, 90 °C.

Scheme 3. Synthesis of Xanthene BACE Inhibitors 10a and 11a[a]

10a (S) R = propyl   **10** (rac) R = propyl
11a (S) R = isobutyl   **11** (rac) R = isobutyl
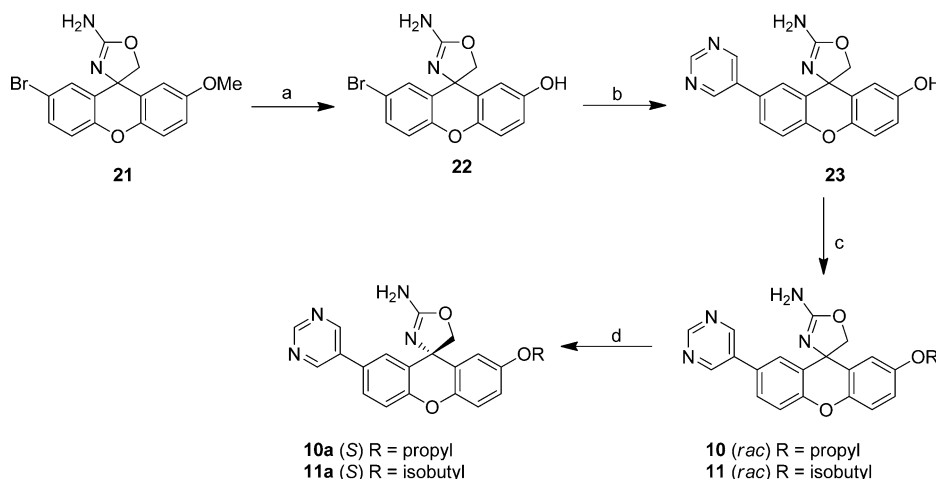
[a]Reagents: (a) BBr$_3$, CH$_2$Cl$_2$, 23 °C, 85%; (b) pyrimidin-5-ylboronic acid, Pd(PPh$_3$)$_4$, K$_2$CO$_3$, THF−H$_2$O, 100 °C, 64%; (c) alkyl iodide (RI), Cs$_2$CO$_3$, DMF; (d) chiral HPLC.

Aminooxazoline xanthenes were synthesized according to the route outlined in Scheme 2. Diaryl ether **18** was prepared by copper-catalyzed etherification of aryl bromide **17**.[32] Subsequent Friedel−Crafts acylation provided xanthenone **19** which was converted to the terminal olefin **20** by a Peterson-type olefination.[33] The addition of in situ generated iodine isocyanate to the olefin followed by treatment with ammonium hydroxide led to 2-aminooxazoline aryl bromide **21**.[34] Suzuki coupling of aryl bromide **21** with a variety of arylboronic acids generated the desired 2-aminooxazoline xanthenes **9**.

As shown in Scheme 3, the 2-aminooxazoline xanthene ether analogues **10a** and **11a** were accessed in three steps from intermediate **21**. Boron tribromide mediated demethylation of bromide **21** cleanly yielded phenol **22**. A subsequent Suzuki coupling provided **23**. Selective alkylation of the phenol with alkyl iodides then afforded the desired alkoxyxanthenes. It is noteworthy that there were minimal N-alkylated products observed under these conditions. Subsequent chiral separation furnished optically pure enantiomers **10a** and **11a**.

CONCLUSION

A structure- and property-based approach led to the discovery of aminooxazoline xanthenes as potent and selective BACE inhibitors. Optimized compound **11a** demonstrated good cellular potency while maintaining properties necessary for penetration across the blood−brain barrier. A single oral dose of **11a** produced a significant Aβ$_{40}$ reduction in the CNS in naive rats. Development and characterization of this series of BACE inhibitors for the treatment of AD will be the subject of future publications.

EXPERIMENTAL SECTION

BACE1 Enzymatic Assay. BACE1 enzymatic activity was determined by the enhancement of fluorescence intensity upon enzymatic cleavage of the fluorescence resonance energy transfer substrate. The BACE1 recognition and cleavage sequence of the substrate are derived from the reported literature,[25a] and the fluorophore and quencher dyes are attached to the side chain of Lys residues at the termini of the substrate peptide. The human recombinant BACE1[35] assay was performed in 50 mM acetate, pH 4.5, 8% DMSO, 100 μM Genepol, 0.002% Brij-35. In dose-response IC$_{50}$ assays, 10 point 1:3 serial dilutions of compound in DMSO were preincubated with the enzyme for 60 min at room temperature. Subsequently, the substrate was added to initiate the reaction. After 60 min at room temperature, the reaction was stopped by addition of 0.1 M Tris base to raise the pH above the enzyme active range, and the increase of fluorescence intensity was measured on Safire II microplate reader (Tecan, Männedorf, Switzerland).

Cell-Based Assay. Human embryonic kidney cells (HEK293) stably expressing APP$_{SW}$ were plated at a density of 100K cells/well in

96-well plates (Costar). The cells were cultivated for 6 h at 37 °C and 5% CO_2 in DMEM supplemented with 10% FBS. Cells were incubated overnight with test compounds at concentrations ranging from 0.0005 to 10 μM. Following incubation with the test compounds the conditioned medium was collected and the Aβ40 levels were determined using a sandwich ELISA. The IC_{50} was calculated from the percent of control Aβ40 as a function of the concentration of the test compound. The sandwich ELISA to detect Aβ40 was performed in 96-well microtiter plates, which were precoated with goat anti-rabbit IgG (Pierce). The capture and detection antibody pair that was used to detect Aβ40 from cell supernatants consists of affinity purified pAβ40 (Invitrogen) and biotinylated 6E10 (Covance), respectively. Conditioned medium was incubated with capture antibody overnight at 4 °C followed by washing. The detecting antibody incubation was for 3 h at 4 °C, again followed by the wash steps as described previously. The plate was developed using Delfia reagents (streptavidin–europium and enhancement solution (Perkin-Elmer)), and time-resolved fluorescence was measured on an EnVision multilabel plate reader (Perkin-Elmer).

Permeability Assay. The wild type cell line LLC-PK1 (porcine renal epithelial cells, WT-LLC-PK1) was purchased from American Type Culture Collection (ATCC, Manassass, VA). Transfections of WT-LLC-PK1 cells with human *MDR*1 gene (hMDR1-LLC-PK1) and rat *mdr1a* gene (rMdr1a-LLC-PK1) were generated. Cells were grown in medium 199 supplemented with 10% fetal bovine serum.[36] Cells were seeded onto Matrigel-coated Transwell filter membranes at a density of 90 000 cells/well. Change of medium was performed on day 3. Compound incubations were performed 5–6 days after seeding. All cultures were incubated at 37 °C in a humidified (95% relative humidity) atmosphere of 5% CO_2/95% air.

Prior to the transport experiment,[37] culture medium was aspirated from both apical and basolateral wells, and cells were rinsed with warmed (37 °C) Hank's balanced salt solution supplemented with 10 mM Hepes at pH 7.4 (HHBSS, Invitrogen, Grand Island, NY). HHBSS was removed from wells prior to dosing with test drugs at 5 μM in transport buffer (HHBSS containing 0.1% bovine serum albumin). An amount of 150 μL of transport buffer was added to receiver chambers prior to dosing in triplicate to apical or basolateral chambers. The dosed Transwell plates containing the cell monolayers were incubated for 2 h at 37 °C on a shaking platform. At the end of the incubation period, 100 μL samples were collected from receiver reservoirs and analyzed by LC–MS/MS on an API4000 (Applied Biosystem, Foster City, CA) triple quadruple mass spectrometer interfaced with TurboIonSpray operated in positive mode using Analyst 1.4.2 software.

The apparent permeability coefficient (P_{app}) of all tested agents was estimated from the slope of a plot of cumulative amount of the agent versus time based on the following equation:

$$P_{app} = (dQ/dt)/(AC_0)$$

where dQ/dt is the penetration rate of the agent (ng/s), A is the surface area of the cell layer on the Transwell (0.11 cm^2), and C_0 is the initial concentration of the test compound (ng/mL). Efflux ratio (ER) was calculated from the basolateral-to-apical permeability divided by the apical-to-basolateral permeability: $ER = [P_{app}(B \rightarrow A)]/[P_{app}(A \rightarrow B)]$.

Microsomal Stability Assay. Compounds (1 μM) were incubated with liver microsomes (0.25 mg/mL in 67 mM phosphate buffer, pH 7.4) from human and rat at 37 °C for 30 min with or without 1 mM NADPH in a total volume of 0.2 mL. The final concentration of DMSO in the incubation was <0.1%. Incubations were stopped by addition of 200 μL of ice-cold acetonitrile containing 0.5% formic acid and an internal standard (500 ng/mL) followed by centrifugation at 3100 rpm for 20 min. The supernatants were analyzed directly (without any further sample cleanup) by high performance liquid chromatography (HPLC) and mass spectrometric detection.

X-ray Crystal Structure. The catalytic domain of human BACE1 (residues 14–453) was overexpressed in *E. coli* and refolded from inclusion bodies following a procedure described previously.[25b]

Inhibitor complexes were obtained by soaking apo BACE crystals in mother liquor solutions supplemented with 1 mM compound for a period of 6–14 h. Crystals were transferred briefly into a cryosolution consisting of 25% (w/v) PEG 5000 MME, 0.1 M sodium citrate (pH 6.6), 0.2 M ammonium iodide, and 20% (v/v) glycerol prior to being flash frozen in liquid nitrogen. Diffraction data were collected on a FRE rotating anode X-ray source equipped with an RAXIS IV++ detector, and images were processed using the HKL suite of programs.[38] The structures were solved by molecular replacement with AMORE using 1W50 as a search model, and they were refined using REFMAC.[39] Model building was performed with COOT.[40] Data collection and refinement statistics appear in the Supporting Information.

Pharmacodynamic Assay. Male Sprague–Dawley rats (175–200 g) were purchased from Harlan and were maintained on a 12 h light/dark cycle with unrestricted access to food and water until use. Rats were administered compound by oral gavage at the appropriate dose. Rats were euthanized with CO_2 inhalation for 2 min, and cisterna magna was quickly exposed by removing the skin and muscle above it. CSF (50–100 μL) was collected with a 30 gauge needle through the dura membrane covering the cisterna magna. Blood was withdrawn by cardiac puncture and plasma obtained by centrifugation for drug exposures. Brains were removed and, along with the CSF, immediately frozen on dry ice and stored at −80 °C until use. The frozen brains were subsequently homogenized in 10 volumes of (w/v) of 0.5% Triton X-100 in TBS with protease inhibitors. The homogenates were centrifuged at 100 000 rpm for 30 min at 4 °C. The supernatants were analyzed for Aβ40 levels by immunoassay as follows: Meso Scale 96-well avidin plates were coated with biotin-4G8 (Covance) and detected with ruthenium-labeled Fab specific for Aβ40. Plates were read in an MSD Sector6000 imager according to the manufacturer's recommended protocol (Meso Scale Discovery, Inc.). Aβ40 concentrations were plotted using Graphpad Prism and analyzed by one-way ANOVA followed by Dunnett's multiple comparison analysis to compare drug-treated animals to vehicle-treated controls.

Chemistry. Unless otherwise noted, all materials were obtained from commercial suppliers and used without further purification. Anhydrous solvents were obtained from Aldrich and used directly. All reactions involving air- or moisture-sensitive reagents were performed under a nitrogen or argon atmosphere. All final compounds were purified to ≥95% purity as determined by high-performance liquid chromatography (HPLC). Purity was measured using Agilent 1100 series HPLC systems with UV detection at 254 nm. System A had the following parameters: Agilent Zorbax Eclipse XDB-C8 4.6 mm × 150 mm, 5 μm, 5–100% CH_3CN in H_2O with 0.1% TFA for 15 min at 1.5 mL/min. System B had the following parameters: Zorbax SB-C8, 4.6 mm × 75 mm, 10–90% CH_3CN in H_2O with 0.1% formic acid for 12 min at 1.0 mL/min. Silica gel columns were used with prepacked silica gel cartridges (Biotage). ^{1}H NMR spectra were recorded on a Bruker AV-400 (400 MHz) spectrometer or on a Bruker AV-500 (500 MHz) spectrometer at ambient temperature. NMR spectra were processed using ACD SpecManager (version 12; ACD, Toronto, Canada). All observed protons are reported as parts per million (ppm) downfield from tetramethylsilane (TMS) or other internal reference in the appropriate solvent indicated. Data are reported as follows: chemical shift, multiplicity (s = singlet, d = doublet, t = triplet, q = quartet, br = broad, m = multiplet), coupling constants, and number of protons. Melting points were determined on a TA Instruments Q200 DSC (New Castle, DE, U.S.). Low-resolution mass spectrometry (MS) data were determined on an Agilent 1100 series LCMS with UV detection at 254 nm and a low resonance electrospray mode (ESI). Exact mass confirmation was performed on an Agilent 1200 series HPLC system (Santa Clara, CA, U.S.) by flow injection analysis, and elution was with binary solvent systems A and B (A, water with 0.1% FA; B, ACN with 0.1% FA) under gradient conditions (5–95% B over 3 min) at 0.3 mL/min with MS detection by an Agilent 6510-Q-TOF mass spectrometer (Santa Clara, CA, U.S.).

Representative Synthetic Protocols of the Aminooxazolines Shown in Schemes 1–3. Exemplified Analogues of Scheme 1. Preparation of 4-(4-(Difluoromethoxy)phenyl)-4-(3-(2-fluoro-

pyridin-3-yl)phenyl)-4,5-dihydrooxazol-2-amine (7). *Step a.* To a solution of (3-bromophenyl)(4-methoxyphenyl)methanone (4.00 g, 14 mmol) in DCM (69 mL) at 0 °C was added boron tribromide (21 mL, 21 mmol) dropwise. The resulting reaction mixture was warmed to room temperature and stirred overnight. After the mixture was stirred overnight, the reaction was not complete as indicated by LCMS. An additional 21 mL of BBr$_3$ (1 M) was added. The mixture was stirred for an additional 24 h. Saturated aqueous NaHCO$_3$ was added slowly to quench the reaction mixture at room temperature. The mixture was then transferred to a separatory funnel, and the aqueous layer was extracted with EtOAc. The organic layers were combined, dried over MgSO$_4$, filtered, and concentrated in vacuo to an oil. The product was purified by chromatography on silica gel (0−100% 90:10:1 DCM/MeOH/NH$_4$OH in DCM) to yield (3-bromophenyl)(4-hydroxyphenyl)methanone (2.9 g, 76% yield). ^{1}H NMR (400 MHz, CDCl$_3$) δ 8.19−8.23 (m, 1H), 8.03 (ddd, J = 1.03, 1.79, 7.95 Hz, 1H), 7.87−7.91 (m, 1H), 7.83 (ddd, J = 1.03, 1.96, 7.97 Hz, 1H), 7.75−7.80 (m, 1H), 7.69 (dddd, J = 1.08, 1.83, 7.86, 13.00 Hz, 1H), 7.39−7.45 (m, 1H), 7.33−7.39 (m, 1H), 6.91−6.96 (m, 1H). MS m/z = 277.2 [M + H]$^+$.

Steps b and c. To a solution of (3-bromophenyl)(4-hydroxyphenyl)methanone (2.89 g, 10.4 mmol), potassium carbonate (6.49 g, 46.9 mmol), and water (2.10 mL) in DMF (20.9 mL) was added 2-chloro-2,2-difluoroacetic acid (2.64 mL, 31.3 mmol) dropwise. After gas ceased to evolve, the reaction vessel was sealed and heated to 100 °C. This mixture was stirred overnight and then transferred to a separatory funnel containing water. The aqueous layer was extracted with DCM. The organic layers were combined, dried over MgSO$_4$, filtered, and concentrated in vacuo to an oil. The crude product was purified by chromatography on silica gel (0−100% 90:10:1 DCM/MeOH/NH$_4$OH in DCM) to provide (3-bromophenyl)(4-(difluoromethoxy)phenyl)methanone (2.4 g, 70% yield). MS m/z 327.3 [M + H]$^+$. To a solution of methyltriphenylphosphonium bromide (3.7 g, 10 mmol) in THF (25 mL) at 0 °C was added n-BuLi (5.5 mL, 8.8 mmol) dropwise. After the mixture was stirred at 0 °C for 30 min, a solution of (3-bromophenyl)(4-(difluoromethoxy)phenyl)methanone (2.4 g, 7.3 mmol) in THF (9.2 mL) was added dropwise. The solution was allowed to warm to room temperature and stirred for 1 h and 15 min. The reaction mixture was quenched with water, and the aqueous layer was extracted with EtOAc. The combined organic layers were dried over MgSO$_4$, filtered, and concentrated in vacuo to an oil. The crude product was purified by chromatography on silica gel (0−30% EtOAc in hexanes) to provide 1-bromo-3-(1-(4-(difluoromethoxy)phenyl)-vinyl)benzene (2.35 g, 99% yield). ^{1}H NMR (400 MHz, CDCl$_3$) δ 7.41 (t, J = 1.66 Hz, 1H), 7.33−7.37 (m, 1H), 7.14−7.19 (m, 3H), 7.11 (dd, J = 6.70, 7.80 Hz, 1H), 5.33 (d, J = 0.98 Hz, 1H), 5.26 (d, J = 1.08 Hz, 1H), 3.74 (s, 3H). MS m/z = 325.2 [M + H]$^+$.

Steps d and e. To a solution of 1-bromo-3-(1-(4-(difluoromethoxy)phenyl)vinyl)benzene (2.4 g, 7.2 mmol) in Et$_2$O (18 mL, 7.2 mmol) was added cyanatosilver (3.2 g, 22 mmol) at room temperature. The resulting mixture was cooled to −6 °C. Solid iodine (1.8 g, 7.2 mmol) was added in one portion, and the solution was stirred for 4 h. The solution was then filtered through a cotton/Celite plug and concentrated in vacuo to an oil. The crude mixture was taken forward to the following step without further purification. MS m/z = 493.5 [M + H]$^+$. To a solution of the crude 1-bromo-3-(1-(4-(difluoromethoxy)phenyl)-2-iodo-1-isocyanatoethyl)benzene (3.6 g, 7.2 mmol) in acetone (22 mL, 7.2 mmol) at room temperature was added ammonium hydroxide (30% in water) (2.52 mL, 22 mmol) by syringe. The resulting mixture was stirred overnight. The reaction mixture was partitioned between water and DCM, and the aqueous layer was extracted with DCM. The combined organic extracts were dried over MgSO$_4$, filtered, and concentrated in vacuo to an oil. The product was purified by chromatography on silica gel (0−40% 90:10:1 DCM/MeOH/NH$_4$OH in DCM). The enantiomers of the purified racemic product were separated by chiral chromatography [5 μm Chiralcel OJ (4.6 mm × 100 mm) under SFC conditions with a mobile phase of 10% methanol with 0.2% diethylamine in CO$_2$ and a flow rate of 5 mL/min] to provide 1.1 g of the (R)-4-(3-bromo-4-fluorophenyl)-4-(4-methoxyphenyl)-4,5-dihydrooxazol-2-amine and

1.0 g of the (S)-4-(3-bromo-4-fluorophenyl)-4-(4-methoxyphenyl)-4,5-dihydrooxazol-2-amine. The overall yield was 75% for two steps. ^{1}H NMR (400 MHz, CDCl$_3$) δ 7.45−7.53 (m, 2H), 7.31−7.38 (m, 2H), 7.20−7.30 (m, 3H), 7.08−7.16 (m, 2H), 6.75 (t, J = 73.75 Hz, 1H), 5.49 (d, J = 0.78 Hz, 1H), 5.48 (d, J = 0.88 Hz, 1H). MS m/z = 383.1 [M + H]$^+$.

Step f. (R)-4-(3-Bromo-4-fluorophenyl)-4-(4-methoxyphenyl)-4,5-dihydrooxazol-2-amine (0.070 g, 0.18 mmol) was added to a vial followed by DME (1.0 mL). The vial was kept under a stream of argon, and 2-fluoro-3-pyridineboronic acid (0.051 g, 0.37 mmol), Pd(PPh$_3$)$_4$ (0.047 g, 0.037 mmol), and sodium carbonate (2.0 M, 0.40 mL) were added. The vial was capped and heated to 125 °C for 16 h. The reaction mixture was cooled to room temperature and concentrated in vacuo. The crude product was purified by RPHPLC using 0.1% formic acid in acetonitrile and water as the mobile phase. (R)-4-(4-(Difluoromethoxy)phenyl)-4-(3-(2-fluoropyridin-3-yl)-phenyl)-4,5-dihydrooxazol-2-amine (0.046 g, 58% yield) was isolated as a white solid. ^{1}H NMR (400 MHz, DMSO-d_6) δ 8.19−8.29 (m, 1H), 8.15 (s, 1H), 8.07 (ddd, J = 1.91, 7.46, 10.29 Hz, 1H), 7.69 (br s, 1H), 7.40−7.56 (m, 6H), 6.96−7.39 (m, 3H), 4.72−4.86 (m, 2H). MS m/z = 400.2 [M + H]$^+$.

Exemplified Analogues of Scheme 2. Preparation of 2′-Methoxy-7′-(pyrimidin-5-yl)-5H-spiro[oxazole-4,9′-xanthen]-2-amine 2,2,2-Trifluoroacetate (9t). *Step a.* 4-Bromophenol (8.7 g, 50 mmol), Cs$_2$CO$_3$ (16 g, 50 mmol), CuOTf−toluene complex (2:1) (150 mg, 0.625 mmol), and EtOAc (0.25 mL) were added to a solution of 2-bromo-5-methoxybenzoic acid (11.6 g, 50 mmol) in toluene (40 mL) in a sealed tube. The reaction mixture was purged with N$_2$ and heated to 110 °C until the aryl halide was consumed as determined by LCMS (48 h). After cooling to room temperature, the mixture was filtered through a Celite plug. The Celite plug was washed with EtOAc. The mixture was acidified with 1 N HCl and extracted with EtOAc. The combined organic extracts were washed with brine, dried over MgSO$_4$, filtered, and concentrated in vacuo. The residue was purified via column chromatography on silica gel (0−10% MeOH in DCM) to afford 2-(4-bromophenoxy)-5-methoxybenzoic acid (11 g, 68% yield). ^{1}H NMR (400 MHz, CDCl$_3$) δ 7.67 (d, J = 3.23 Hz, 1H), 7.49 (d, J = 9.00 Hz, 1H), 7.49 (dd, J = 5.48, 15.45 Hz, 1H), 7.09 (dd, J = 3.28, 9.05 Hz, 1H), 6.93 (d, J = 9.00 Hz, 1H), 6.93 (dd, J = 5.48, 15.36 Hz, 1H), 6.88 (d, J = 9.00 Hz, 1H), 3.87 (s, 3H). MS m/z = 324.9 [M + H]$^+$.

Step b. Sulfuric acid (0.5M, 41 mL, 21 mmol) was added to 2-(4-bromophenoxy)-5-methoxybenzoic acid (3.75 g, 12 mmol) at room temperature. The reaction mixture was stirred at 60 °C for 1 h. LCMS showed complete reaction. The reaction mixture was cooled to room temperature and poured slowly over a stirred mixture of ice and water (100 mL). The tan precipitate was filtered and washed with water (3 × 30 mL), 0.5 N NaOH (2 × 30 mL), and water again. The residue was recrystallized from 40 mL of THF to give 2-bromo-7-methoxy-9H-xanthen-9-one (2.96 g, 84% yield). ^{1}H NMR (400 MHz, CDCl$_3$) δ 8.48 (dd, J = 0.29, 2.54 Hz, 1H), 7.80 (dd, J = 2.54, 8.90 Hz, 1H), 7.70 (d, J = 3.13 Hz, 1H), 7.46 (dd, J = 0.39, 9.10 Hz, 1H), 7.41 (dd, J = 0.29, 8.90 Hz, 1H), 7.37 (dd, J = 3.13, 9.10 Hz, 1H), 3.94 (s, 3H). MS m/z = 305.2.

Step c. A solution of 2-bromo-7-methoxy-9H-xanthen-9-one (2.04 g, 6.7 mmol) in THF (67 mL) contained in a 250 mL round-bottom flask was cooled in a dry ice/acetone bath for 10 min to give a milky white mixture. Trimethylsilylmethyllithium (10 mL of a 1.0 M solution in pentane, 10 mmol) was added dropwise over 5 min to give a clear orange solution. The mixture was stirred for 15 min. Then acetyl chloride (0.76 mL, 11 mmol) was added dropwise, resulting in the formation of a clear, bright-yellow solution. The mixture was warmed to room temperature for 3 h. Then an additional portion of acetyl chloride (0.25 mL) was added. The mixture was stirred for an additional 30 min before being diluted with saturated aqueous sodium bicarbonate solution (100 mL). The biphasic mixture was extracted with EtOAc (2 × 50 mL), and the combined organic extracts were dried over MgSO$_4$, filtered, and evaporated to give 2-bromo-7-methoxy-9-methylene-9H-xanthene as a yellow solid that was used without further purification. ^{1}H NMR (400 MHz, CDCl$_3$) δ 7.84 (d, J

= 2.25 Hz, 1H), 7.39 (dd, J = 2.35, 8.80 Hz, 1H), 7.16 (d, J = 2.93 Hz, 1H), 7.05−7.09 (m, 1H), 7.01 (d, J = 8.80 Hz, 1H), 6.92 (dd, J = 2.93, 8.90 Hz, 1H), 5.50 (s, 2H), 3.86 (s, 3H). MS m/z = 303.0 [M + H]$^+$.

Step d. Crude 2-bromo-7-methoxy-9-methylene-9*H*-xanthene was suspended in Et$_2$O (33 mL). Silver cyanate (3.0 g, 20 mmol) and iodine (1.7 g, 6.7 mmol) were added in sequence, resulting in a brown mixture. After being stirred for 40 min at room temperature, the reaction mixture was filtered through Celite with the aid of Et$_2$O, and the filtrate was evaporated. The residue was dissolved in a mixture of THF (26 mL) and ammonium hydroxide (2.6 mL), and the mixture was stirred for 15 h. The reaction mixture was partitioned between water (100 mL) and DCM (70 mL). The layers were separated, and the aqueous layer was extracted with DCM (2 × 70 mL). The combined organic extracts were dried over MgSO$_4$, filtered, and evaporated. The residue was purified by chromatography on silica gel (0−40% 90:10:1 DCM/MeOH/NH$_4$OH in DCM) to provide 2′-bromo-7′-methoxyspiro[1,3-oxazole-4,9′-xanthen]-2-amine (1.65 g, 69% yield) as a pale yellow foam. ^{1}H NMR (400 MHz, CDCl$_3$) δ 7.49 (d, J = 2.25 Hz, 1H), 7.41 (dd, J = 2.35, 8.71 Hz, 1H), 7.05 (dd, J = 0.34, 8.75 Hz, 1H), 6.99 (d, J = 8.71 Hz, 1H), 6.86−6.92 (m, 2H), 6.49 (br s, 2H), 4.48 (d, J = 8.80 Hz, 1H), 4.43 (d, J = 8.80 Hz, 1H), 3.82 (s, 3H). MS m/z = 361.2 [M + H]$^+$.

Step e. A 10 mL resealable tube was charged with tetrakis-(triphenylphosphine)palladium (122 mg, 105 μmol) and 5-pyrimidinylboronic acid (98 mg, 789 μmol). A solution of 2′-bromo-7′-methoxyspiro[1,3-oxazole-4,9′-xanthen]-2-amine (190 mg, 526 μmol) in 3 mL of dioxane was added, and the resulting mixture was flushed for 30 s with argon. Sodium carbonate (789 μL, 1578 μmol) (2 M aqueous solution) was added, and the reaction mixture was stirred at 90 °C for 18 h. The resulting mixture was partitioned between water and DCM. The aqueous layer was extracted with DCM. The organic layers were combined, washed with brine, dried over MgSO$_4$, and concentrated in vacuo. The residue was purified by RPHPLC (column, Xbridge 19 mm × 100 mm, 10 μm; flow rate 40 mL/min; mobile phase 0.1% TFA in ACN and water) to afford 2′-methoxy-7′-(pyrimidin-5-yl)-5*H*-spiro[oxazole-4,9′-xanthen]-2-amine 2,2,2-trifluoroacetate (**9t**) (90 mg, 47% yield). Mp 220.3−222.9 °C. ^{1}H NMR (500 MHz, DMSO-d_6) δ 11.25 (br s, 1H), 9.61 (br s, 1H), 9.43 (br s, 1H), 9.24 (s, 2H), 9.21 (s, 1H), 8.20 (d, J = 2.14 Hz, 1H), 7.95 (dd, J = 2.19, 8.60 Hz, 1H), 7.41 (d, J = 8.65 Hz, 1H), 7.29 (d, J = 8.98 Hz, 1H), 7.15 (dd, J = 2.94, 9.03 Hz, 1H), 6.98 (d, J = 2.88 Hz, 1H), 5.14 (s, 2H), 3.82 (s, 3H). HRMS m/z = 361.1293 [M + H]$^+$. Calcd for C$_{20}$H$_{17}$N$_4$O$_3$: 361.1300.

Exemplified Analogues of Scheme 3. 2′-Propoxy-7′-(5-pyrimidinyl)spiro[1,3-oxazole-4,9′-xanthen]-2-amine (10a). *Step a.* A solution of 2′-bromo-7′-methoxyspiro[1,3-oxazole-4,9′-xanthen]-2-amine (1.034 g, 2863 μmol) in DCM (29 mL) contained in a 100 mL round-bottom flask was cooled in an ice bath for 15 min. A solution of boron tribromide (8.5 mL of a 1.0 M solution in DCM, 8.59 mmol) was added dropwise over 5 min, resulting in a dark brown solution. The ice bath was removed, and the mixture was stirred for 1.5 h. The reaction mixture was carefully quenched with saturated aqueous sodium bicarbonate solution (30 mL). The mixture was partitioned between water (50 mL) and DCM (50 mL). The aqueous layer was extracted with DCM (2 × 25 mL), and the combined organic extracts were dried over MgSO$_4$. The solution was filtered, and the filter cake was washed with 10% MeOH/DCM. The combined filtrates were concentrated in vacuo. The residue was purified by chromatography on silica gel (0−70% 90:10:1 DCM/MeOH/NH$_4$OH in DCM) to give 2′-bromo-7′-hydroxyspiro[1,3-oxazole-4,9′-xanthen]-2-amine (845 mg, 85.1% yield). ^{1}H NMR (400 MHz, DMSO-d_6) δ 9.34 (br s, 1H), 7.46 (dd, J = 2.54, 8.71 Hz, 1H), 7.37 (d, J = 2.35 Hz, 1H), 7.08 (d, J = 8.70 Hz, 1H), 6.97 (d, J = 9.00 Hz, 1H), 6.67−6.76 (m, 2H), 6.51 (br s, 2H), 4.10 (d, J = 8.41 Hz, 1H), 4.07 (d, J = 8.41 Hz, 1H). MS m/z = 347.0 [M + H]$^+$.

Step b. A 150 mL pressure vessel was charged with 2′-bromo-7′-hydroxyspiro[1,3-oxazole-4,9′-xanthen]-2-amine (845 mg, 0.243 mmol) in THF (24 mL), pyrimidin-5-ylboronic acid (754 mg, 6085 μmol), tetrakis(triphenylphosphine)palladium(0) (281 mg, 243 μmol), and potassium carbonate (10.1 mL of a 1.2 M aqueous

solution, 12.1 mmol). The vessel was sealed and placed in a 100 °C oil bath for 4 h. The reaction mixture was cooled to room temperature and partitioned between EtOAc (50 mL) and water (50 mL). The aqueous layer was extracted with EtOAc (2 × 50 mL), and the combined organic extracts were dried over MgSO$_4$, filtered, and evaporated. The crude material was purified by chromatography on silica gel (30−100% 90:10:1 DCM/MeOH/NH$_4$OH in DCM) to give 2′-hydroxy-7′-(5-pyrimidinyl)spiro[1,3-oxazole-4,9′-xanthen]-2-amine (538 mg, 64% yield) as an off-white solid. ^{1}H NMR (400 MHz, DMSO-d_6) δ 9.35 (br s, 1H), 9.17 (s, 1H), 9.08 (s, 2H), 7.73 (dd, J = 2.30, 8.46 Hz, 1H), 7.65 (d, J = 2.25 Hz, 1H), 7.26 (d, J = 8.41 Hz, 1H), 7.00 (d, J = 8.71 Hz, 1H), 6.68−6.79 (m, 2H), 6.45 (br s, 2H), 4.22 (d, J = 8.31 Hz, 1H), 4.17 (d, J = 8.22 Hz, 1H). MS m/z = 347.2 [M + H]$^+$.

Step c. A glass vial was charged with 2′-hydroxy-7′-(5-pyrimidinyl)-spiro[1,3-oxazole-4,9′-xanthen]-2-amine (53.7 mg, 155 μmol), cesium carbonate (75.7 mg, 232 μmol), DMF (0.62 mL), and 1-iodopropane (16.6 μL, 170 μmol). The mixture was stirred at room temperature for 18 h, then poured into water (10 mL) and extracted with EtOAc (3 × 7 mL). The combined organic extracts were dried over MgSO$_4$, filtered, and evaporated. The residue was purified by chromatography on silica gel (0−80% 90:10:1 DCM/MeOH/NH$_4$OH in DCM) to give 2′-(1-propyloxy)-7′-(5-pyrimidinyl)spiro[1,3-oxazole-4,9′-xanthen]-2-amine (55.0 mg, 91.4% yield) as a white solid. ^{1}H NMR (400 MHz, DMSO-d_6) δ 9.18 (s, 1H), 9.08 (s, 2H), 7.75 (dd, J = 2.30, 8.46 Hz, 1H), 7.67 (d, J = 2.25 Hz, 1H), 7.28 (d, J = 8.51 Hz, 1H), 7.12 (d, J = 8.90 Hz, 1H), 6.93 (dd, J = 3.03, 8.90 Hz, 1H), 6.83 (d, J = 3.03 Hz, 1H), 6.45 (br s, 2H), 4.23 (ABq, J = 8.31 Hz, 2H), 3.84 − 3.98 (m, 2H), 1.68−1.79 (m, 2H), 0.99 (t, J = 7.43 Hz, 3H). HRMS m/z = 389.1618 [M + H]$^+$. Calcd for C$_{22}$H$_{21}$N$_4$O$_3$: 389.1613.

Step d. 2′-Propoxy-7′-(5-pyrimidinyl)spiro[1,3-oxazole-4,9′-xanthen]-2-amine (40 mg) was subjected to chromatography using 15:85:0.2 MeOH/CO$_2$/DEA at 80 mL/min on a 20 mm × 250 mm, 5 μm ChiralPak AS-H column and 100 bar system pressure. The first peak (t_R =3.5 min) corresponded to (*R*)-2′-propoxy-7′-(5-pyrimidinyl)spiro[1,3-oxazole-4,9′-xanthen]-2-amine (13.0 mg, >99% ee), and the second peak (t_R =4.3 min) corresponded to (*S*)-2′-propoxy-7′-(5-pyrimidinyl)spiro[1,3-oxazole-4,9′-xanthen]-2-amine (12.8 mg, >99% ee).

■ ASSOCIATED CONTENT

Ⓢ Supporting Information

Experimental details, analytical data, and X-ray crystallographic information for cocrystals of BACE + **6**, BACE + **9l**, and BACE + **11a**. This material is available free of charge via the Internet at http://pubs.acs.org.

Accession Codes

The PDB accession codes for the X-ray cocrystal structures of BACE + **6**, BACE + **9l**, and BACE + **11a** are 4FRI, 4FRJ, and 4FRK, respectively.

■ AUTHOR INFORMATION

Corresponding Author

*For H.H.: phone, 617-444-5197; fax, 617-621-3908; e-mail, hongbing.huang@amgen.com. For D.S.L.: phone, 617-444-5187; fax, 617-621-3908; e-mail, daniel.la@amgen.com.

Present Address

△Sanofi-Aventis, 270 Albany Street, Cambridge, Massachusetts 02139, United States.

Author Contributions

∞These authors contributed equally to the rational design of the aminooxazoline xanthene structure.

Notes

The authors declare no competing financial interest.

■ ABBREVIATIONS USED

AD, Alzheimer's disease; Aβ, β-amyloid peptide; APP, β-amyloid precursor protein; BACE1, β-site β-amyloid precursor protein cleaving enzyme; CNS, central nervous system; CSF, cerebrospinal fluid; FRET, fluorescence resonance energy transfer; HE, hydroxyethylene; HEA, hydroxyethylamine; Pgp, p-glycoprotein

■ REFERENCES

(1) (a) Cummings, J. L. Biomarkers in Alzheimer's disease drug development. *Alzheimer's Dementia* **2011**, 7 (3), e13−e44. (b) Cummings, J. L. Alzheimer's disease. *N. Engl. J. Med.* **2004**, 351 (1), 56−67. (c) Citron, M. Alzheimer's disease: strategies for disease modification. *Nat. Rev. Drug Discovery* **2010**, 9 (5), 387−98. (d) Jakob-Roetne, R.; Jacobsen, H. Alzheimer's disease: from pathology to therapeutic approaches. *Angew Chem., Int. Ed.* **2009**, 48 (17), 3030−3059.

(2) (a) Medina, M. Recent developments in tau-based therapeutics for neurodegenerative diseases. *Recent Pat. CNS Drug Discovery* **2011**, 6 (1), 20−30. (b) Mattson, M. P. Pathways towards and away from Alzheimer's disease. *Nature* **2004**, 430 (7000), 631−639. (c) Nussbaum, R. L.; Ellis, C. E. Alzheimer's disease and Parkinson's disease. *N. Engl. J. Med.* **2003**, 348 (14), 1356−1364. (d) Selkoe, D. J. Translating cell biology into therapeutic advances in Alzheimer's disease. *Nature* **1999**, 399 (6738 Suppl.), A23−A31.

(3) (a) Checler, F.; Turner, A. J. *Journal of Neurochemistry* special issue on Alzheimer's disease: "amyloid cascade hypothesis—20 years on". *J. Neurochem.* **2012**, 120 (Suppl. 1), iii−iv. (b) Armstrong, R. A. The pathogenesis of Alzheimer's disease: a reevaluation of the "amyloid cascade hypothesis". *Int. J. Alzheimer's Dis.* **2011**, 2011, 630865. (c) Cummings, J. Alzheimer's disease: clinical trials and the amyloid hypothesis. *Ann. Acad. Med. Singapore* **2011**, 40 (7), 304−303. (d) Sinha, S.; Lieberburg, I. Cellular mechanisms of beta-amyloid production and secretion. *Proc. Natl. Acad. Sci. U.S.A.* **1999**, 96 (20), 11049−11053.

(4) (a) Wang, Z.; Yang, L.; Zheng, H. Role of APP and Abeta in synaptic physiology. *Curr. Alzheimer Res.* **2012**, 9 (2), 217−226. (b) Chasseigneaux, S.; Allinquant, B. Functions of Abeta, sAPPalpha and sAPPbeta: similarities and differences. *J. Neurochem.* **2012**, 120 (Suppl. 1), 99−108. (c) Guo, Q.; Li, H.; Gaddam, S. S.; Justice, N. J.; Robertson, C. S.; Zheng, H. Amyloid precursor protein revisited: neuron-specific expression and highly stable nature of soluble derivatives. *J. Biol. Chem.* **2012**, 287 (4), 2437−2445. (d) Farah, M. H.; Pan, B. H.; Hoffman, P. N.; Ferraris, D.; Tsukamoto, T.; Nguyen, T.; Wong, P. C.; Price, D. L.; Slusher, B. S.; Griffin, J. W. Reduced BACE1 activity enhances clearance of myelin debris and regeneration of axons in the injured peripheral nervous system. *J. Neurosci.* **2011**, 31 (15), 5744−5754. (e) Nikolaev, A.; McLaughlin, T.; O'Leary, D. D.; Tessier-Lavigne, M. APP binds DR6 to trigger axon pruning and neuron death via distinct caspases. *Nature* **2009**, 457 (7232), 981−989.

(5) (a) Cho, J. E.; Kim, J. R. Recent approaches targeting beta-amyloid for therapeutic intervention of Alzheimer's disease. *Recent Pat. CNS Drug Discovery* **2011**, 6 (3), 222−233. (b) Ganjei, J. K. Targeting amyloid precursor protein secretases: Alzheimer's disease and beyond. *Drug News Perspect.* **2010**, 23 (9), 573−584. (c) Silvestri, R. Boom in the development of non-peptidic beta-secretase (BACE1) inhibitors for the treatment of Alzheimer's disease. *Med. Res. Rev.* **2009**, 29 (2), 295−338. (d) Albert, J. S. Progress in the development of beta-secretase inhibitors for Alzheimer's disease. *Prog. Med. Chem.* **2009**, 48, 133−161. (e) Guo, T.; Hobbs, D. W. Development of BACE1 inhibitors for Alzheimer's disease. *Curr. Med. Chem.* **2006**, 13 (15), 1811−1829.

(6) (a) Luo, Y.; Bolon, B.; Kahn, S.; Bennett, B. D.; Babu-Khan, S.; Denis, P.; Fan, W.; Kha, H.; Zhang, J.; Gong, Y.; Martin, L.; Louis, J. C.; Yan, Q.; Richards, W. G.; Citron, M.; Vassar, R. Mice deficient in BACE1, the Alzheimer's beta-secretase, have normal phenotype and abolished beta-amyloid generation. *Nat. Neurosci.* **2001**, 4 (3), 231−232. (b) Cai, H.; Wang, Y.; McCarthy, D.; Wen, H.; Borchelt, D. R.; Price, D. L.; Wong, P. C. BACE1 is the major beta-secretase for generation of Abeta peptides by neurons. *Nat. Neurosci.* **2001**, 4 (3), 233−234. (c) Roberds, S. L.; Anderson, J.; Basi, G.; Bienkowski, M. J.; Branstetter, D. G.; Chen, K. S.; Freedman, S. B.; Frigon, N. L.; Games, D.; Hu, K.; Johnson-Wood, K.; Kappenman, K. E.; Kawabe, T. T.; Kola, I.; Kuehn, R.; Lee, M.; Liu, W.; Motter, R.; Nichols, N. F.; Power, M.; Robertson, D. W.; Schenk, D.; Schoor, M.; Shopp, G. M.; Shuck, M. E.; Sinha, S.; Svensson, K. A.; Tatsuno, G.; Tintrup, H.; Wijsman, J.; Wright, S.; McConlogue, L. BACE knockout mice are healthy despite lacking the primary beta-secretase activity in brain: implications for Alzheimer's disease therapeutics. *Hum. Mol. Genet.* **2001**, 10 (12), 1317−1324.

(7) Ghosh, A. K.; Brindisi, M.; Tang, J. Developing beta-secretase inhibitors for treatment of Alzheimer's disease. *J. Neurochem.* **2012**, 120 (Suppl. 1), 71−83.

(8) (a) Safety Study of CTS21166 To Treat Alzheimer Disease. http://clinicaltrials.gov/ct2/show/NCT00621010 (accessed April 2012). (b) Drahl, C. Beta Testing. *Chem. Eng. News* **2010**, 88, 14.

(9) (a) Huang, X. P.; Chang, W. P.; Koelsch, G.; Turner, R. T., 3rd; Lupu, F.; Tang, J. Internalization of exogenously added memapsin 2 (beta-secretase) ectodomain by cells is mediated by amyloid precursor protein. *J. Biol. Chem.* **2004**, 279 (36), 37886−37894. (b) He, X.; Cooley, K.; Chung, C. H.; Dashti, N.; Tang, J. Apolipoprotein receptor 2 and X11 alpha/beta mediate apoliprotein E-induced endocytosis of amyloid-beta precursor protein and beta-secretase, leading to amyloid-beta production. *J. Neurosci.* **2007**, 27 (15), 4052−4060. (c) Rajendran, L.; Schneider, A.; Schlechtingen, G.; Weidlich, S.; Ries, J.; Braxmeier, T.; Schwille, P.; Schulz, J. B.; Schroeder, C.; Simons, M.; Jennings, G.; Knolker, H. J.; Simons, K. Efficient inhibition of the Alzheimer's disease beta-secretase by membrane targeting. *Science* **2008**, 320 (5875), 520−523.

(10) (a) Vassar, R.; Bennett, B. D.; Babu-Khan, S.; Kahn, S.; Mendiaz, E. A.; Denis, P.; Teplow, D. B.; Ross, S.; Amarante, P.; Loeloff, R.; Luo, Y.; Fisher, S.; Fuller, J.; Edenson, S.; Lile, J.; Jarosinski, M. A.; Biere, A. L.; Curran, E.; Burgess, T.; Louis, J. C.; Collins, F.; Treanor, J.; Rogers, G.; Citron, M. Beta-secretase cleavage of Alzheimer's amyloid precursor protein by the transmembrane aspartic protease BACE. *Science* **1999**, 286 (5440), 735−741. (b) Yan, R.; Bienkowski, M. J.; Shuck, M. E.; Miao, H.; Tory, M. C.; Pauley, A. M.; Brashier, J. R.; Stratman, N. C.; Mathews, W. R.; Buhl, A. E.; Carter, D. B.; Tomasselli, A. G.; Parodi, L. A.; Heinrikson, R. L.; Gurney, M. E. Membrane-anchored aspartyl protease with Alzheimer's disease beta-secretase activity. *Nature* **1999**, 402 (6761), 533−537. (c) Sinha, S.; Anderson, J. P.; Barbour, R.; Basi, G. S.; Caccavello, R.; Davis, D.; Doan, M.; Dovey, H. F.; Frigon, N.; Hong, J.; Jacobson-Croak, K.; Jewett, N.; Keim, P.; Knops, J.; Lieberburg, I.; Power, M.; Tan, H.; Tatsuno, G.; Tung, J.; Schenk, D.; Seubert, P.; Suomensaari, S. M.; Wang, S.; Walker, D.; Zhao, J.; McConlogue, L.; John, V. Purification and cloning of amyloid precursor protein beta-secretase from human brain. *Nature* **1999**, 402 (6761), 537−540.

(11) Stachel, S. J. Progress toward the development of a viable BACE inhibitor. *Drug Dev. Res.* **2009**, 70, 101−110.

(12) (a) Cole, D. C.; Manas, E. S.; Stock, J. R.; Condon, J. S.; Jennings, L. D.; Aulabaugh, A.; Chopra, R.; Cowling, R.; Ellingboe, J. W.; Fan, K. Y.; Harrison, B. L.; Hu, Y.; Jacobsen, S.; Jin, G.; Lin, L.; Lovering, F. E.; Malamas, M. S.; Stahl, M. L.; Strand, J.; Sukhdeo, M. N.; Svenson, K.; Turner, M. J.; Wagner, E.; Wu, J.; Zhou, P.; Bard, J. Acylguanidines as small-molecule beta-secretase inhibitors. *J. Med. Chem.* **2006**, 49 (21), 6158−6161. (b) Edwards, P. D.; Albert, J. S.; Sylvester, M.; Aharony, D.; Andisik, D.; Callaghan, O.; Campbell, J. B.; Carr, R. A.; Chessari, G.; Congreve, M.; Frederickson, M.; Folmer, R. H.; Geschwindner, S.; Koether, G.; Kolmodin, K.; Krumrine, J.; Mauger, R. C.; Murray, C. W.; Olsson, L. L.; Patel, S.; Spear, N.; Tian,

G. Application of fragment-based lead generation to the discovery of novel, cyclic amidine beta-secretase inhibitors with nanomolar potency, cellular activity, and high ligand efficiency. *J. Med. Chem.* **2007**, *50* (24), 5912−5925. (c) Congreve, M.; Aharony, D.; Albert, J.; Callaghan, O.; Campbell, J.; Carr, R. A.; Chessari, G.; Cowan, S.; Edwards, P. D.; Frederickson, M.; McMenamin, R.; Murray, C. W.; Patel, S.; Wallis, N. Application of fragment screening by X-ray crystallography to the discovery of aminopyridines as inhibitors of beta-secretase. *J. Med. Chem.* **2007**, *50* (6), 1124−1132. (d) Baxter, E. W.; Conway, K. A.; Kennis, L.; Bischoff, F.; Mercken, M. H.; Winter, H. L.; Reynolds, C. H.; Tounge, B. A.; Luo, C.; Scott, M. K.; Huang, Y.; Braeken, M.; Pieters, S. M.; Berthelot, D. J.; Masure, S.; Bruinzeel, W. D.; Jordan, A. D.; Parker, M. H.; Boyd, R. E.; Qu, J.; Alexander, R. S.; Brenneman, D. E.; Reitz, A. B. 2-Amino-3,4-dihydroquinazolines as inhibitors of BACE-1 (beta-site APP cleaving enzyme): use of structure based design to convert a micromolar hit into a nanomolar lead. *J. Med. Chem.* **2007**, *50* (18), 4261−4264. (e) Malamas, M. S.; Erdei, J.; Gunawan, I.; Turner, J.; Hu, Y.; Wagner, E.; Fan, K.; Chopra, R.; Olland, A.; Bard, J.; Jacobsen, S.; Magolda, R. L.; Pangalos, M.; Robichaud, A. J. Design and synthesis of 5,5′-disubstituted amino-hydantoins as potent and selective human beta-secretase (BACE1) inhibitors. *J. Med. Chem.* **2010**, *53* (3), 1146−1158.

(13) Cole, D. C.; Bursavich, M. G. Nonpeptide BACE 1 Inhibitors: Design and Synthesis. In *Methods and Principles in Medicinal Chemistry*; Ghosh, A. K., Ed.; Wiley-VCH: Weinheim, Germany, 2010; Vol. *45*, pp 481−509.

(14) The Asp binding moiety would act as the pharmacaphore and therefore be implemented into every compound henceforth. Thus, this portion required the heaviest physiochemical design restrictions. Wager, T. T.; Villalobos, A.; Verhoest, P. R.; Hou, X.; Shaffer, C. L. Strategies to optimize the brain availability of central nervous system drug candidates. *Expert Opin. Drug Discovery* **2011**, *6*, 371−381.

(15) Hitchcock, S. A.; Pennington, L. D. Structure−brain exposure relationships. *J. Med. Chem.* **2006**, *49* (26), 7559−7583.

(16) pK_a values were calculated using the following: *ACD LogD Suite*, version 10; Advanced Chemistry Development Inc.: Toronto, Canada.

(17) Benchmark compounds synthesized containing cores B and H demonstrated efflux ratios of >40.

(18) Rajamani, R.; Reynolds, C. H. Modeling the protonation states of the catalytic aspartates in beta-secretase. *J. Med. Chem.* **2004**, *47* (21), 5159−5166.

(19) (a) Sidera, C.; Liu, C.; Austen, B. Pro-domain removal in ASP-2 and the cleavage of the amyloid precursor are influenced by pH. *BMC Biochem.* **2002**, *3*, 25. (b) Dominguez, J. L.; Christopeit, T.; Villaverde, M. C.; Gossas, T.; Otero, J. M.; Nystrom, S.; Baraznenok, V.; Lindstrom, E.; Danielson, U. H.; Sussman, F. Effect of the protonation state of the titratable residues on the inhibitor affinity to BACE-1. *Biochemistry* **2010**, *49* (34), 7255−7263.

(20) (a) Stachel, S. J.; Coburn, C. A.; Rush, D.; Jones, K. L.; Zhu, H.; Rajapakse, H.; Graham, S. L.; Simon, A.; Katharine Holloway, M.; Allison, T. J.; Munshi, S. K.; Espeseth, A. S.; Zuck, P.; Colussi, D.; Wolfe, A.; Pietrak, B. L.; Lai, M. T.; Vacca, J. P. Discovery of aminoheterocycles as a novel beta-secretase inhibitor class: pH dependence on binding activity part 1. *Bioorg. Med. Chem. Lett.* **2009**, *19* (11), 2977−2980. (b) Rajapakse, H. A.; Nantermet, P. G.; Selnick, H. G.; Barrow, J. C.; McGaughey, G. B.; Munshi, S.; Lindsley, S. R.; Young, M. B.; Ngo, P. L.; Holloway, M. K.; Lai, M. T.; Espeseth, A. S.; Shi, X. P.; Colussi, D.; Pietrak, B.; Crouthamel, M. C.; Tugusheva, K.; Huang, Q.; Xu, M.; Simon, A. J.; Kuo, L.; Hazuda, D. J.; Graham, S.; Vacca, J. P. SAR of tertiary carbinamine derived BACE1 inhibitors: role of aspartate ligand amine pKa in enzyme inhibition. *Bioorg. Med. Chem. Lett.* **2010**, *20* (6), 1885−1889.

(21) Reynolds, D. P.; Lanevskij, K.; Japertas, P.; Didziapetris, R.; Petrauskas, A. Ionization-specific analysis of human intestinal absorption. *J. Pharm. Sci.* **2009**, *98* (11), 4039−4054.

(22) (a) Kotthaus, J.; Hungeling, H.; Reeh, C.; Schade, D.; Wein, S.; Wolffram, S.; Clement, B. Synthesis and biological evaluation of L-valine-amidoximeesters as double prodrugs of amidines. *Bioorg. Med. Chem.* **2011**, *19* (6), 1907−1914. (b) Peterlin-Masic, L.; Cesar, J.;

Zega, A. Metabolism-directed optimisation of antithrombotics: the prodrug principle. *Curr. Pharm. Des* **2006**, *12* (1), 73−91.

(23) Kaller, M. R.; Harried, S. S.; Albrecht, B.; Amarante, P.; Babu-Khan, S.; Bartberger, M. D.; Brwon, J.; Brown, R.; Chen, K.; Cheng, Y.; Citron, M.; Croghan, M. D.; Graceffa, R.; Hickman, D.; Judd, T.; Kriemen, C.; La, D.; Li, V.; Lopez, P.; Luo, Y.; Masse, C.; Monenschein, H.; Nguyen, T.; Pennington, L. D.; Miguel, T. S.; Sickmier, E. A.; Wahl, R. C.; Weiss, M. M.; Wen, P. H.; Williamson, T.; Wood, S.; Xue, M.; Yang, B.; Zhang, J.; Patel, V.; Zhong, W.; Hitchcock, S. A potent and orally efficacious, hydroxyethylamine-based inhibitor of β-secretase. *ACS Med. Chem. Lett.* [Online early access]. DOI: 10.1021/ml3000148. Published Online: April 22, **2012**.

(24) (a) Ward, J. M.; Gorenstein, N. M.; Tian, J.; Martin, S. F.; Post, C. B. Constraining binding hot spots: NMR and molecular dynamics simulations provide a structural explanation for enthalpy-entropy compensation in SH2-ligand binding. *J. Am. Chem. Soc.* **2010**, *132* (32), 11058−11070. (b) Schneider, H.-J. In *Protein−Ligand Interactions: From Molecular Recognition to Drug Design*; Böhm, H.-J., Schneider, G., Eds; Wiley-VCH: Weinheim, Germany, 2003; pp 21−50.

(25) (a) Turner, R. T., 3rd; Koelsch, G.; Hong, L.; Castanheira, P.; Ermolieff, J.; Ghosh, A. K.; Tang, J. Subsite specificity of memapsin 2 (beta-secretase): implications for inhibitor design. *Biochemistry* **2001**, *40* (34), 10001−10006. (b) Patel, S.; Vuillard, L.; Cleasby, A.; Murray, C. W.; Yon, J. Apo and inhibitor complex structures of BACE (beta-secretase). *J. Mol. Biol.* **2004**, *343* (2), 407−416.

(26) Hong, L.; Turner, R. T., 3rd; Koelsch, G.; Shin, D.; Ghosh, A. K.; Tang, J. Crystal structure of memapsin 2 (beta-secretase) in complex with an inhibitor OM00-3. *Biochemistry* **2002**, *41* (36), 10963−10967.

(27) (a) Stachel, S. J.; Coburn, C. A.; Steele, T. G.; Jones, K. G.; Loutzenhiser, E. F.; Gregro, A. R.; Rajapakse, H. A.; Lai, M. T.; Crouthamel, M. C.; Xu, M.; Tugusheva, K.; Lineberger, J. E.; Pietrak, B. L.; Espeseth, A. S.; Shi, X. P.; Chen-Dodson, E.; Holloway, M. K.; Munshi, S.; Simon, A. J.; Kuo, L.; Vacca, J. P. Structure-based design of potent and selective cell-permeable inhibitors of human beta-secretase (BACE-1). *J. Med. Chem.* **2004**, *47* (26), 6447−6450. (b) Coburn, C. A.; Stachel, S. J.; Li, Y. M.; Rush, D. M.; Steele, T. G.; Chen-Dodson, E.; Holloway, M. K.; Xu, M.; Huang, Q.; Lai, M. T.; DiMuzio, J.; Crouthamel, M. C.; Shi, X. P.; Sardana, V.; Chen, Z.; Munshi, S.; Kuo, L.; Makara, G. M.; Annis, D. A.; Tadikonda, P. K.; Nash, H. M.; Vacca, J. P.; Wang, T. Identification of a small molecule nonpeptide active site beta-secretase inhibitor that displays a nontraditional binding mode for aspartyl proteases. *J. Med. Chem.* **2004**, *47* (25), 6117−6119.

(28) van de Waterbeemd, H.; Camenisch, G.; Folkers, G.; Chretien, J. R.; Raevsky, O. A. Estimation of blood−brain barrier crossing of drugs using molecular size and shape, and H-bonding descriptors. *J. Drug Targeting* **1998**, *6* (2), 151−165.

(29) (a) Obach, R. S. Nonspecific binding to microsomes: impact on scale-up of in vitro intrinsic clearance to hepatic clearance as assessed through examination of warfarin, imipramine, and propranolol. *Drug Metab. Dispos.* **1997**, *25* (12), 1359−1369. (b) Obach, R. S. Prediction of human clearance of twenty-nine drugs from hepatic microsomal intrinsic clearance data: an examination of in vitro half-life approach and nonspecific binding to microsomes. *Drug Metab. Dispos.* **1999**, *27* (11), 1350−1359. (c) Smith, D. A.; van de Waterbeemd, H.; Walker, D. K. In *Pharmacokinetics and Metabolishm in Drug Design*; Mannhold, R., Kubinyi, H., Folkers, G., Eds; Wiley-VCH: Weinheim, Germany, 2006; pp 165−177.

(30) The relatively low clearance of **11a** is likely a result of high plasma protein binding. The protein binding in rat plasma for **9u** and **11a** is 98% and 91.3%, respectively.

(31) Dineen, T. A.; Weiss, M. M.; Williamson, T.; Acton, P.; Babu-Khan, S.; Bartberger, M. D.; Brown, J.; Chen, K.; Cheng, Y.; Citron, M.; Croghan, M. D.; Dunn, R. T., 2nd; Esmay, J.; Graceffa, R. F.; Harried, S. S.; Hickman, D.; Hitchcock, S. A.; Horne, D. B.; Huang, H.; Imbeah-Ampiah, R.; Judd, T.; Kaller, M. R.; Kreiman, C. R.; La, D. S.; Li, V.; Lopez, P.; Louie, S.; Monenschein, H.; Nguyen, T. T.; Pennington, L. D.; San Miguel, T.; Sickmier, E. A.; Vargas, H. M.;

Wahl, R. C.; Wen, P. H.; Whittington, D. A.; Wood, S.; Xue, Q.; Yang, B. H.; Patel, V. F.; Zhong, W. Design and synthesis of potent, orally efficacious hydroxyethylamine derived beta-site amyloid precursor protein cleaving enzyme (BACE1) inhibitors. *J. Med. Chem.* [Online early access]. DOI: 10.1021/jm300118s. Published Online: April 18, **2012**.

(32) Marcoux, J.; Doye, S; Buchwald, S. L. A general copper-catalyzed syntesis of diaryl ethers. *J. Am. Chem. Soc.* **1997**, *119*, 10539–10540.

(33) Peterson, D. J. Carbonyl olefination reaction using silyl-substituted organometallic compounds. *J. Org. Chem.* **1968**, *33*, 780–784.

(34) Fernandez, J. M. G.; Mellet, C. O.; Adrian, M. A. P.; Mota, J. F. Syntheses and spectral properties of *β*-iodoureas and 2-amino-4,4-diphenyl-2-oxazolines. *J. Heterocycl. Chem.* **1991**, *28*, 777–780.

(35) Haniu, M.; Denis, P.; Young, Y.; Mendiaz, E. A.; Fuller, J.; Hui, J. O.; Bennett, B. D.; Kahn, S.; Ross, S.; Burgess, T.; Katta, V.; Rogers, G.; Vassar, R.; Citron, M. Characterization of Alzheimer's beta-secretase protein BACE. A pepsin family member with unusual properties. *J. Biol. Chem.* **2000**, *275* (28), 21099–21106.

(36) Schinkel, A. H.; Wagenaar, E.; van Deemter, L.; Mol, C. A.; Borst, P. Absence of the mdr1a P-glycoprotein in mice affects tissue distribution and pharmacokinetics of dexamethasone, digoxin, and cyclosporin A. *J. Clin. Invest.* **1995**, *96* (4), 1698–1705.

(37) Booth-Genthe, C. L.; Louie, S. W.; Carlini, E. J.; Li, B.; Leake, B. F.; Eisenhandler, R.; Hochman, J. H.; Mei, Q.; Kim, R. B.; Rushmore, T. H.; Yamazaki, M. Development and characterization of LLC-PK1 cells containing Sprague-Dawley rat Abcb1a (Mdr1a): comparison of rat P-glycoprotein transport to human and mouse. *J. Pharmacol. Toxicol. Methods* **2006**, *54* (1), 78–89.

(38) Otwinowski, Z.; Minor, W. Processing of X-ray diffraction data collected in oscillation mode. *Methods Enzymol.* **1997**, *276*, 307–326.

(39) (a) Navaza, J. AMoRe: an automated package for molecular replacement. *Acta Crystallogr. A* **1994**, *50*, 157–163. (b) Murshudov, G. N.; Vagin, A. A.; Dodson, E. J. Refinement of macromolecular structures by the maximum-likelihood method. *Acta Crystallogr., Sect. D: Biol. Crystallogr.* **1997**, *53* (Part 3), 240–255.

(40) Emsley, P.; Cowtan, K. Coot: model-building tools for molecular graphics. *Acta Crystallogr., Sect. D: Biol. Crystallogr.* **2004**, *60*, 2126–2132.